Optimization Methods and Software
Vol. 00, No. 00, January 2012, 1–34

RESEARCH ARTICLE

Optimal Flow Control Based on POD and MPC and an Application to the Cancellation of Tollmien-Schlichting Waves

Jane Ghiglieri[ab*] and Stefan Ulbrich[ab]

[a]*Graduate School of Computational Engineering, Technische Universität Darmstadt, Germany*; [b]*Nonlinear Optimization, Department of Mathematics, Technische Universität Darmstadt, Germany*

(*Received 00 Month 200x; in final form 00 Month 200x*)

A reduced-order model based on Proper Orthogonal Decomposition (POD) is presented which is suitable for active control in fluid dynamical systems. The POD basis is based on snapshots (Finite Element discretizations of the Navier-Stokes equations) of the uncontrolled state and impulse response snapshots. Error estimates for this setting are proved. The reduced set of basis functions is used for active control of fluid flows governed by the Navier-Stokes equations. In particular, we consider the cancellation of Tollmien-Schlichting waves in the boundary layer of a flat plate. The control is a body force induced by a plasma actuator. The optimization of the control parameters is performed within the reduced system with a Model Predictive Control (MPC) approach. The effectiveness of the approach is shown in numerical experiments.

Keywords: Navier-Stokes equations; flow control; model reduction; Proper Orthogonal Decomposition; Model Predictive Control; error estimates

AMS Subject Classification: 49K20, 65K05, 76D55

1. Introduction

Control methods of fluid dynamical systems have received an increasing amount of attention in the last years. In particular for real-time applications, instead of solving a high-dimensional system, a low-order model description is used to perform the optimization. The design of the reduced-order controller depends on the construction of a reduced order description of the flow model and the optimization of the control parameters is performed within the reduced system.

Currently, a widely used and successful model reduction technique is Proper Orthogonal Decomposition (POD). It has served in many cases as a promising model reduction tool for simulation purposes, see e.g. [1, 12, 17, 21, 35].

The required POD basis is based on snapshots, which are solutions of Finite Element discretizations of the Navier-Stokes equations. The quality of the approach highly depends on the chosen snapshot set. The POD may be sufficient to reproduce the dynamics of the flow for a fixed system, but may suffer when the system is under the action of a control. There is no guarantee that the reduced order control problem will converge to the optimal control of the original (large) system.

*Corresponding author. Email: ghiglieri@gsc.tu-darmstadt.de

ISSN: 1055-6788 print/ISSN 1029-4937 online

DOI: 10.1080/1055.6788.YYYY.xxxxxx
http://www.tandfonline.com

The POD method has been applied to flow control, e.g. in [1, 2, 28, 29, 32]. There are techniques introduced to enlarge the computational database in order to accurately capture the system behavior for various control trajectories during optimization. In most of these techniques an adaptive procedure is used to generate new snapshots, which is costly. We propose a combined snapshot ensemble of the uncontrolled state and impulse response snapshots, which can be generated beforehand and is applicable to optimal control problems. Thus, the problem of unmodelled dynamics in the POD approach can be avoided.

Based on POD approximations in space with this special snapshot ensemble and a semi-implicit Euler discretization in time, we extend the techniques used in [22, 23] to obtain an a-priori error estimate. Due to the choice of the snapshot ensemble we can quantify the approximation properties of POD based schemes under control.

The presented paper explores the possibility of developing POD-based reduced-order models for active control of fluid flows governed by the Navier-Stokes equations. In particular, we consider the cancellation of Tollmien-Schlichting waves in the boundary layer of a flat plate. Plasma actuators are considered for flow control. These actuators induce a body force, that leads to a fluid acceleration, such that the velocity profile is changed next to the surface. By optimal control of the plasma actuator parameters it is possible to reduce or even cancel the Tollmien-Schlichting waves, see e.g. [13, 20].

We perform the optimization of the control parameters within the reduced system with a Model Predictive Control (MPC) approach. The efficiency of the reduced-order controller is demonstrated for the damping of Tollmien-Schlichting waves by plasma actuators.

The structure of the paper is as follows. In section 2 the optimal control problem is introduced and the underlying analysis is given in section 3. The Finite Element method is reviewed in section 4. In section 5 we present POD and its properties. We apply POD to the optimal control problem to derive a reduced-order optimal control problem. Additionally, we discuss approaches to adapt the POD reduced-order model to control and we introduce our approach to choose the snapshot ensemble, so that we can finally develop an error estimate in section 6. We review the MPC approach in section 7 and describe our numerical procedure to solve the optimal control problem. In section 8 we present computational results for the optimal control problem and we conclude the paper with section 9.

2. The optimal control problem

In this section we describe the optimal control problem of the cancellation of Tollmien-Schlichting waves by plasma actuators which serves as a model problem. The results presented in this paper are applicable to more general control problems.

2.1. *Configuration*

We consider a specific simulation configuration which was set up to closely resemble an actual experimental configuration employed in several experimental and numerical studies targeting active flow control, e.g. [11, 13], which also includes the cancellation of Tollmien-Schlichting waves. A schematic of the configuration is given in (Figure 1). A planar solid body, a plate, is installed parallel to the flow in the wind tunnel.

The Tollmien-Schlichting waves are seeded into the boundary layer by a plasma

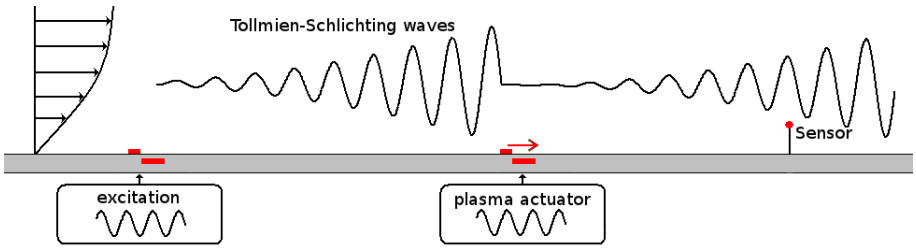

Figure 1. Schematic of the configuration.

actuator operated in pulsed mode, which will result in continuous, mono-frequency waves. This establishes a controlled transition, which is necessary for the experiments as well as for the numerical simulations.

The body force induced by a second plasma actuator is used to manipulate the transition process in the boundary layer. The actuator accelerates the fluid in the lower parts of the boundary layer close to the surface, which leads to a modified boundary-layer profile.

A plasma actuator consists of two electrodes separated by an insulating layer. An AC voltage is applied to the electrodes. As a result an electric field is generated and the air above the actuator is ionized, i.e. the neutral air molecules are broken down into their loaded components: electrons and positive ions. This gaseous state, where free charge carriers are present, is known as plasma. The charged particles are accelerated and a body force is generated above the actuator. For a better insight into the physical background and the working principle of a plasma actuator, see [20].

The result of the excitation and attenuation is recorded 50 mm downstream of the actuator, where a sensor measures the flow velocity above the plate. This position was chosen to allow enough time for a complete interaction of the control force with the Tollmien-Schlichting waves.

2.2. *Control Problem*

In this section we will describe the flow system in detail. We consider a two-dimensional viscous incompressible flow in the domain depicted in (Figure 2).

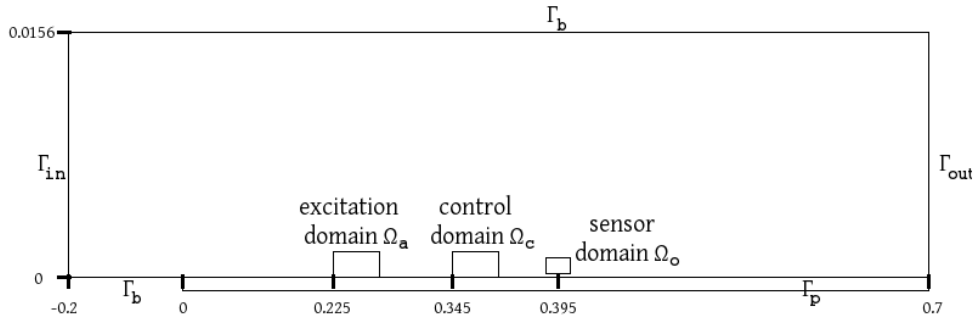

Figure 2. Computational domain

The governing equations are the two-dimensional Navier-Stokes equations.

The flow in the bounded domain $\Omega \subset \mathbb{R}^2$, is characterized by the velocity field $y : \Omega \times [0,T] \to \mathbb{R}^2$ and by the pressure $p : \Omega \times [0,T] \to \mathbb{R}$. The time-dependent

Navier-Stokes equations are given by

$$\begin{aligned} y_t - \nu\Delta y + (y\cdot\nabla)y + \nabla p &= f \qquad \text{in } \Omega\times(0,T] \\ \nabla\cdot y &= 0 \qquad \text{in } \Omega\times(0,T]. \end{aligned} \tag{1}$$

The viscosity of the fluid is given by a parameter $\nu > 0$, the kinetic viscosity.

The artificial excitation of the Tollmien-Schlichting waves is obtained by a plasma actuator operated in pulsed mode. The frequency is $fre = 110$ Hz with a duty cycle of $DC = 50$ %. This results in a body force

$$f_a(x,t) = \begin{cases} f_a(x) & \text{if } \mathrm{mod}(t, \frac{1}{fre}) \le DC\cdot\frac{1}{fre} \\ 0 & \text{otherwise} \end{cases}$$

with a given fixed body force $f_a(x)$ that describes a typical body force distribution of a plasma actuator on Ω_a.

The control action is affected by the plasma actuator acting on Ω_c, a small region above the actuator. Let $f_c : [0,T]\times\Omega \to \mathbb{R}^2$ be the body force acting on the fluid. The force has the form

$$f_c(u;x,t) = u(t)\cdot g(x), \quad \mathrm{supp}(g) = \Omega_c \tag{2}$$

with a time-dependent amplitude $u : [0,T] \to \mathbb{R}$ and a location-dependent field g, describing the spatial distribution of the body force on Ω_c.

At $t = 0$ the initial condition

$$y(\cdot,0) = y_0 \qquad \text{in } \Omega \tag{3}$$

is imposed, where $y_0 : \Omega \to \mathbb{R}^2$ is a given velocity.

Next we describe the boundary conditions. At the inflow boundary Γ_{in} and the boundary part Γ_b, referring to the top and the region right before the plate, we prescribe the Dirichlet condition

$$y(\cdot,t) = y_b \qquad \text{on } \Gamma_{in}\cup\Gamma_b. \tag{4}$$

At the outflow boundary a do-nothing boundary condition

$$\nu\partial_\eta y = p\eta \qquad \text{on } \Gamma_{out} \tag{5}$$

is imposed. Here η denotes the unit normal to $\partial\Omega$ in the outward direction.

At the wall of the flat plate Γ_p the no-slip condition ($y = 0$) is imposed.

The control objective consists in the cancellation of the Tollmien-Schlichting waves.

Tollmien-Schlichting waves induce unsteady fluctuations in the flow velocity. Therefore the velocity values in a fixed spatial point describe a wave over time. The velocity can be measured by a sensor as described in the experimental setup. The signal of the velocity sensor is used to analyze the downstream amplitude of the Tollmien-Schlichting wave. The sensor signal $y_1(x,t)$ describes the velocity in flow direction at time t at position x.

As cost function J we choose the following function

$$J_T(y,u) = \int_0^T \left(\frac{d}{dt}\int_{\Omega_o} y_1(x,t)dx\right)^2 dt + \frac{\alpha}{2}\int_0^T |u(t)|^2 dt. \tag{6}$$

The first part is a measure for the variation of the velocity in the sensor area Ω_o. The second summand weights the costs for the control.

Combining (1) and (3)-(6), we can state the optimal control problem

$$\begin{aligned} &\min \quad J_T(y,u) \\ &\text{subject to} \\ &\qquad y_t - \nu\Delta y + (y\cdot\nabla)y + \nabla p = f_a + f_c(u) && \text{in } \Omega\times(0,T] \\ &\qquad \nabla\cdot y = 0 && \text{in } \Omega\times(0,T] \\ &\qquad y(0) = y_0 && \text{in } \Omega \\ &\qquad y = y_b && \text{on } \Gamma_{in}\cup\Gamma_b\times(0,T] \\ &\qquad \nu\partial_\eta u - p\eta = 0 && \text{on } \Gamma_{out}\times(0,T]. \end{aligned} \tag{7}$$

3. Analysis of the optimal control problem

For simplicity, we consider for the analysis of the optimal control problem (7) only the case of Dirichlet conditions, i.e., $\Gamma_{out} = \emptyset$. We assume that $\Omega \subset \mathbb{R}^2$ is a bounded domain with Lipschitz boundary and introduce the Hilbert spaces

$$\begin{aligned} V &:= cl_{H_0^1(\Omega)^2}\{\phi \in C_c^\infty(\Omega)^2 : \nabla\cdot\phi = 0\}, \\ H &:= cl_{L^2(\Omega)^2}\{\phi \in C_c^\infty(\Omega)^2 : \nabla\cdot\phi = 0\}, \quad (u,v)_{H_0^1} = \int_\Omega \nabla u\cdot\nabla v \,\mathrm{dx} \end{aligned}$$

as well as

$$W(I) := \{y \in L^2(I;V) : y_t \in L^2(I;V')\}, \quad I := [0,T].$$

We obtain the Gelfand triple $V \hookrightarrow H = H' \hookrightarrow V'$ with dense embeddings. It is well known that the embedding $W(I) \hookrightarrow C(I;H)$ is continuous. We make the following assumption:

(A1) $\Omega \subset \mathbb{R}^2$ is a bounded domain with Lipschitz boundary. Assume that the Dirichlet data y_b admits an extension $\overline{y} \in H^1(\Omega)$ with $\nabla\cdot\overline{y} = 0$, let $y_0 \in \overline{y} + H$, and let the actuator forces satisfy $f_a \in L^2(I;L^2(\Omega))$, $g \in L^2(\Omega)$, $u \in L^2(I)$.

This implies in particular that $f_c(u) \in L^2(I;L^2(\Omega))$.

We introduce the trilinear form

$$b : H^1(\Omega)^2 \times H^1(\Omega)^2 \times H^1(\Omega)^2 \mapsto \mathbb{R}, \quad b(v,w,\phi) := \langle (v\cdot\nabla)w, \phi\rangle_{(H^1)',H^1}.$$

It is well known that $b(v,w,\phi) = -b(v,\phi,w)$ for all $v,w \in H^1(\Omega)$, $\phi \in H_0^1(\Omega)$ with $\nabla\cdot v = 0$. Moreover,

$$|b(v,w,\phi)| \le 2^{1/2}\|v\|_{L^2}^{1/2}\|v\|_{H_0^1}^{1/2}\|w\|_{H_0^1}\|\phi\|_{L^2}^{1/2}\|\phi\|_{H_0^1}^{1/2} \quad \forall v,w,\phi \in H_0^1(\Omega)^2 \tag{8}$$

and using $H^1(\Omega) \hookrightarrow L^4(\Omega)$ we have for all $v,w,\phi \in H_0^1(\Omega)^2$

$$\begin{aligned} |b(\overline{y}+v,\overline{y}+w,\phi)| &\le 2^{1/2}\|v\|_{L^2}^{1/2}\|v\|_{H_0^1}^{1/2}\|w\|_{H_0^1}\|\phi\|_{L^2}^{1/2}\|\phi\|_{H_0^1}^{1/2} \\ &\quad + c_b\|\overline{y}\|_{H_0^1}(\|\overline{y}\|_{H_0^1} + \|v\|_{H_0^1} + \|w\|_{H_0^1})\|\phi\|_{L^2}^{1/2}\|\phi\|_{H_0^1}^{1/2}. \end{aligned}$$

In the case $\Gamma_{out} = \emptyset$ a weak solution y of the constraints in (7) is defined as follows. Find $y \in \overline{y} + W(I)$ such that for all $\phi \in V$, a.e. on I

$$\begin{aligned} \langle y_t, \phi \rangle_{V',V} + b(y, y, \phi) + \nu(\nabla y, \nabla \phi)_{L^2(\Omega)} = (f_a + f_c(u), \phi)_{L^2(\Omega)} \\ y(0, \cdot) = y_0. \end{aligned} \tag{9}$$

This defines with the spaces

$$Y := W(I), \quad U := L^2(I), \quad Z := L^2(I; V') \times H$$

the operator

$$\begin{aligned} &E : Y \times U \mapsto Z, \\ &E(y - \overline{y}, u) = \begin{pmatrix} y_t + b(y, y, \cdot) + \nu(\nabla y, \nabla \cdot)_{L^2} - f_a - f_c(u) \\ y(\cdot, 0) - y_0 \end{pmatrix} \text{ for } y - \overline{y} \in Y. \end{aligned} \tag{10}$$

We collect several properties of the operator $E(y, u)$.

Proposition 3.1 *Let assumption (A1) hold. Then the following holds for the Navier-Stokes operator E in (10).*

1) *$E : Y \times U \mapsto Z$ is infinitely many times Fréchet differentiable.*
2) *For all $(v, u) \in Y \times U$ the derivative $E_v(v, u) \in \mathcal{L}(Y, Z)$ has a bounded inverse.*
3) *For all $u \in U$ the state equation $E(v, u) = 0$ has a unique solution $v = v(u) \in Y$ and $u \in U \mapsto v(u) \in Y$ is bounded as well as infinitely many times Fréchet differentiable.*

Proof For 1) and 3) see, e.g., [16, 18, 34] and for 2) [33] in the case $y_b = 0$, i.e., $\overline{y} = 0$. The extension to the case $\overline{y} \in H^1$, $\nabla \cdot \overline{y} = 0$ is straightforward by the above estimate for b. ■

The objective functional (6) requires a more regular state space. The following assumption ensures an appropriate setting.

(A2) $\Omega \subset \mathbb{R}^2$ is a bounded domain with C^2-boundary or a convex polygon. Assume that the Dirichlet data y_b admits an extension $\overline{y} \in H^2(\Omega)$ with $\nabla \cdot \overline{y} = 0$, let $y_0 \in \overline{y} + V$, and let the actuator forces satisfy $f_a \in L^2(I; L^2(\Omega))$, $g \in L^2(\Omega)$, $u \in L^2(I)$.

Define the spaces

$$Y_1 := \{v \in L^2(I; V \cap H^2(\Omega)^2),\ v_t \in L^2(I; H)\}, \quad Z_1 := L^2(I; H') \times V.$$

Then the imbedding $Y_1 \hookrightarrow C(I; V)$ is continuous and the trilinear form satisfies [33, Lem. III.3.8]

$$b(v, w, \phi) \le c_1 \|v\|_{H^1} \|w\|_{H^1}^{1/2} \|w\|_{H^2}^{1/2} \|\phi\|_H \quad \forall\ v, w \in H^1(\Omega)^2,\ \phi \in H.$$

Hence, we obtain for all $v, w \in Y_1$ and $\phi \in L^2(I; H)$

$$\begin{aligned} \|b(v, w, \phi)\|_{L^1(I)} &\le c_1 \|v\|_{L^\infty(I;V)} \|w\|_{L^2(I;V)}^{1/2} \|w\|_{L^2(I;H^2)}^{1/2} \|\phi\|_{L^2(I;H)} \\ &\le c_1 \|v\|_{Y_1} \|w\|_{Y_1} \|\phi\|_{L^2(I;H)} \end{aligned}$$

and thus, we have $b(v, w, \cdot) \in L^2(I; H')$ as well as $-\Delta v \in L^2(I; H')$. Hence, we can define the operator

$$\begin{aligned} &E : Y_1 \times U \mapsto Z_1, \\ &E(y - \overline{y}, u) = \begin{pmatrix} y_t + b(y, y, \cdot) - \nu\Delta y - f_a - f_c(u) \\ y(\cdot, 0) - y_0 \end{pmatrix} \text{ for } y - \overline{y} \in Y_1. \end{aligned} \tag{11}$$

We have the following variant of Proposition 3.1.

THEOREM 3.2 *Let assumption (A2) hold. Then the following holds for the Navier-Stokes operator E in (11).*

1) *$E : Y_1 \times U \mapsto Z_1$ is infinitely many times Fréchet differentiable.*
2) *For all $(v, u) \in Y_1 \times U$ the derivative $E_v(v, u) \in \mathcal{L}(Y_1, Z_1)$ has a bounded inverse.*
3) *For all $u \in U$ the state equation $E(v, u) = 0$ has a unique solution $v = v(u) \in Y_1$ and $u \in U \mapsto v(u) \in Y_1$ is bounded as well as infinitely many times Fréchet differentiable.*

Proof 1) follows easily from the definition of Y_1, Z_1 and the fact that $b : Y_1 \times Y_1 \times L^2(I; H) \to \mathbb{R}$ is a continuous trilinear form. For 2) see, e.g., [16] in the case of C^2 boundary. The case of a convex polygon can be obtained by the same proof using the H^2 regularity of the Stokes operator, see e.g. [15].

ad 3): For $y_b = 0$ the existence of a unique solution $v(u) \in Y_1$ is shown in [33] for the case of C^2 boundary, see [15] for the case of a convex polygon. The modification for the case $\overline{y} \in H^2(\Omega)^2$, $\nabla \cdot \overline{y} = 0$ is straightforward. By 1) and 2) the implicit function theorem can be applied and yields that $u \in U \mapsto v(u) \in Y_1$ is infinitely many times Fréchet differentiable. ■

We obtain immediately the following result.

LEMMA 3.3 *Let assumption (A2) hold. Then the reduced objective functional $u \in U \mapsto J_T(y(u), u)$ in (6), where $y(u) = \overline{y} + v(u)$ is the unique weak solution of (9), is infinitely many times Fréchet differentiable.*

Proof By the definition of Y_1 it is obvious that $(v, u) \in Y_1 \times U \mapsto J_T(\overline{y} + v, u)$ is infinitely many times Fréchet differentiable. Hence the result follows from Theorem 3.2, 3). ■

We show next that the optimal control problem (7) has an optimal solution.

LEMMA 3.4 *Let $\Gamma_{out} = \emptyset$ and assumption (A2) hold. If $\alpha > 0$ in (6), then the optimal control problem (7) has an optimal solution $(y^*, u^*) \in Y_1 \times U$.*

Proof Let (y^k, u^k) be a minimizing sequence with $J_T(y^k, u^k) \searrow J_T^*$, where J_T^* is the infimum of (7). Then $y^k = y(u^k) = \overline{y} + v(u^k) \in Y_1$ is the unique weak solution of (9). Since $\alpha > 0$ and both terms of J_T are non-negative, we have $\alpha \|u^k\|_U^2 \leq J_T(y^0, u^0) < \infty$. Hence (u^k) is uniformly bounded in U and by the boundedness of $u \in U \mapsto y(u) \in Y_1$ the sequence (y^k, u^k) is uniformly bounded in the Hilbert space $Y_1 \times U$. Hence, we have possibly after choosing a subsequence $(y^k, u^k) \rightharpoonup (y^*, u^*)$ weakly in $Y_1 \times U$. Since $(y, u) \in Y_1 \times U \mapsto J_T(y, u)$ is continuous and convex, it is sequentially weakly lower semicontinuous and therefore $J_T(y^*, u^*) \leq \liminf_{k\to\infty} J_T(y^k, u^k) = J_T^*$. It remains to show that $y^* = y(u^*)$. To this end we have only to consider the nonlinear term $b(y^k, y^k, \phi)$ in (9). Using the fact that $Y_1 \hookrightarrow Y$ and that the embedding $Y \hookrightarrow\hookrightarrow L^2(I; H)$ is compact, we deduce that

$y^k \to y^* \in L^2(I;L^2)$. Now we have for all $w \in L^\infty(I;V)$

$$\begin{aligned} b(y^k,y^k,w) - b(y^*,y^*,w) &= b(y^k-y^*,y^k,w) + b(y^*,y^k-y^*,w) \\ &= b(y^k-y^*,y^k,w) - b(y^*,w,y^k-y^*) \end{aligned}$$

and hence by (8)

$$\begin{aligned} &\int_0^T |b(y^k(t),y^k(t),w) - b(y^*(t),y^*(t),w)|\,dt \leq \\ &\leq 2^{1/2}\|y^k-y^*\|^{1/2}_{L^2(I;H)}\|y^k-y^*\|^{1/2}_{L^2(I;V)}(\|y^k\|_{L^2(I;H^1)} + \|y^*\|_{L^2(I;H^1)})\|w\|_{L^\infty(I;V)} \\ &\leq \text{const.}\|y^k-y^*\|^{1/2}_{L^2(I;H)} \to 0. \end{aligned}$$

Since $L^\infty(I;V)$ is dense in $L^2(I;V)$, this shows that y^* is the unique weak solution $y(u^*)$ of (9). ■

4. Finite Element approximation

In order to apply nonlinear model predictive control techniques for the approximate solution of (7), we will derive a reduced order model of the PDE constraint. It will be based on a Finite Element approximation of (9). For simplicity we consider again the case $\Gamma_{out} = \emptyset$ and assume that Ω is a polyhedral domain.

Let $\mathcal{T}_h = \{K\}$ be a regular triangulation of $\overline{\Omega}$ into closed triangles K, such that each $K \in \mathcal{T}_h$ contains a circle of radius $\kappa_1 h$ and is contained in a circle of radius $\kappa_2 h$, where $0 < \kappa_1 \leq \kappa_2$ are independent of h. We approximate the velocity space $H_0^1(\Omega)^2$ and the pressure space L^2 by the $P_2 - P_1$ Taylor-Hood elements, i.e.,

$$\begin{aligned} H_h &= \{v^h \in C(\overline{\Omega})^2 :\ v^h|_K \in P_2(K)^2\ \forall K \in \mathcal{T}_h\}, \quad H_{h,0} := H_h \cap H_0^1(\Omega)^2, \\ L_h &= \{p^h \in C(\overline{\Omega}) :\ p^h|_K \in P_1(K)\ \forall K \in \mathcal{T}_h\}, \quad L_{h,0} := \{p^h \in L_h :\ \int_\Omega p^h\,dx = 0\}, \end{aligned}$$

where $P_j(K)$ is the space of polynomials with degree $\leq j$. The solenoidal space V is now approximated by

$$V_h = \{v^h \in H_{h,0} :\ (q^h, \nabla\cdot v^h)_{L^2(\Omega)} = 0 \quad \forall\, q^h \in L_{h,0}\}.$$

It is well known that $H_{h,0}$ and $L_{h,0}$ satisfy uniformly in h a discrete inf-sup condition [5, 15] and that the following approximation property holds.

PROPOSITION 4.1 *There exists a constant c_V independent of h such that for all $v \in V \cap H^2(\Omega)^2$*

$$\inf_{v^h \in V_h} \|v - v^h\|_{L^2(\Omega)} + h\|\nabla(v-v^h)\|_{L^2(\Omega)} \leq c_V h^2 \|v\|_{H^2(\Omega)}.$$

Proof See, e.g., [3, 15]. ■

4.1. *Semidiscretization in space*

We consider now the following semidiscretization of (9). Let

$$\overline{y}^h \in H_h, \quad (q^h, \nabla \cdot \overline{y}^h)_{L^2(\Omega)} = 0 \ \ \forall\, q^h \in L_{h,0}, \quad \|\overline{y}^h\|_{H^1(\Omega)} \le c_{\overline{y}} \|\overline{y}\|_{H^1(\Omega)}$$

be an approximation of $\overline{y}$ and set

$$\widehat{b}(v^h, w^h, \phi^h) := \frac{1}{2}(b(v^h, w^h, \phi^h) - b(v^h, \phi^h, w^h)). \tag{12}$$

Find $y^h \in \overline{y}^h + H^1(I; V_h)$ such that

$$\begin{aligned} (y_t^h, \phi^h)_{L^2(\Omega)} + \widehat{b}(y^h, y^h, \phi^h) + \nu(\nabla y^h, \nabla \phi^h)_{L^2(\Omega)} &= (f_a + f_c(u), \phi^h)_{L^2(\Omega)} \\ (y^h(0,\cdot) - y_0, \phi^h)_{L^2(\Omega)} &= 0 \end{aligned} \tag{13}$$

for all $\phi^h \in V_h$, a.e. on I.

We obtain the following a priori error estimate.

LEMMA 4.2 *Let (A2) hold. Then there exists a constant* $c(\|u\|_{L^2}) = c\left(\|f_a + f_c(u)\|_{L^2(I;L^2(\Omega))}, \|y_0\|_{H^1(\Omega)}, \|\overline{y}\|_{H^1(\Omega)}\right)$ *independent of* h *such that*

$$\|y - y^h\|_{L^2(I;H^1)} + \|y - y^h\|_{L^\infty(I;L^2)} \le c(\|u\|_{L^2}) \left(h + \inf_{\phi_h \in V_h} \|\overline{y} - \overline{y}^h - \phi^h\|\right).$$

Proof For a proof in the case $y_b = 0$ see [3, 15]. The extension to the case $\overline{y} \in H^2(\Omega)$ is elementary but technical. We omit the details. ■

4.2. *Discretization in time*

To obtain a fully discrete problem, we apply a semi-implicit Euler method in time.

For $m \in \mathbb{N}$ we introduce the equidistant time grid

$$0 = \tau_0 < \tau_1 < \ldots < \tau_m = T, \quad \delta\tau = \tau_j - \tau_{j-1} \quad \text{for } j = 1, \ldots, m.$$

We now determine $y_k^h \in \overline{y}^h + V_h$, $k = 0, \ldots, m$, by the following scheme

$$\begin{aligned} (y_0^h - y_0, \phi^h)_{L^2(\Omega)} &= 0 \\ (\overline{\partial}_\tau y_k^h, \phi^h)_{L^2(\Omega)} + \widehat{b}(y_{k-1}^h, y_k^h, \phi^h) & \\ +\nu(\nabla y_k^h, \nabla \phi^h)_{L^2(\Omega)} &= (f_a + f_c(u_k), \phi^h)_{L^2(\Omega)} \\ \forall\, \phi_h \in V_h, \ k = 1, \ldots, m. & \end{aligned} \tag{14}$$

Here, we have set

$$\overline{\partial}_\tau y_k^h = \frac{y_k^h - y_{k-1}^h}{\delta\tau}.$$

We write this scheme briefly as: Find $y_k^h \in \overline{y}^h + V_h$ with

$$\begin{aligned} (y_0^h - y_0, \phi^h)_{L^2(\Omega)} &= 0 \\ \left\langle C^{h,k}(y_k^h, y_{k-1}^h), \phi^h \right\rangle_{V_h', V_h} &= (f_a + f_c(u_k), \phi^h)_{L^2(\Omega)} \\ \forall\, \phi^h \in V_h, \quad k = 1, \ldots, m. & \end{aligned} \tag{15}$$

This scheme will form the basis for the construction of a reduced order model based on POD. An a priori error analysis for (14) and for the reduced order model will be carried out in section 6.1.

To abbreviate notation, we introduce the discrete norms

$$\begin{aligned} \|(y_k^h)\|_{L^p(I;X)} &:= \left(\sum_{k=1}^{m} \delta\tau \, \|y_k^h\|_X^p \right)^{1/p}, \ p \in [1, \infty), \\ \|(y_k^h)\|_{L^\infty(I;X)} &:= \max_{1 \le k \le m} \|y_k^h\|_X, \end{aligned} \tag{16}$$

where usually $X = L^2(\Omega)$ or $X = H^1(\Omega)$. This corresponds to the identification of $(y_k^h)_{k=1}^m$ with a function that has the value y_k^h on $(\tau_{k-1}, \tau_k]$.

5. Reduced Order Model

The disretization of the optimal control problem (7) based on scheme (14) leads to a very large-scale nonlinear optimization problem. Model reduction can help to reduce the dimension of the problem significantly. The obtained low-dimensional model should guarantee a reasonable performance while being computationally tractable.

We consider a Reduced Order Model (ROM) approach that approximates the nonlinear dynamics by a Galerkin technique. Instead of the Finite Element space V_h in (14), it utilizes a low-dimensional space spanned by basis functions that contain characteristics of the expected controlled flow. Various ROM techniques differ in the choice of the basis functions. We focus on POD for the low-order description of the flow model and the optimization will be performed with the resulting reduced system.

5.1. *Proper Orthogonal Decomposition*

The POD Galerkin projection method has already successfully been applied when dealing with the Navier-Stokes equations, see [1, 12, 17, 21, 27, 35] for example.

Here we briefly outline the snapshot variant of POD introduced by Sirovich in [31] to obtain a low-dimensional approximation of the Navier-Stokes equations. In this variant the construction of the POD basis is based on the information contained in snapshots, which provide the state solution of the dynamical system at pre-specified time instances. While other methods, like the Finite Element method, use basis functions that have little connection to the problem or to the underlying partial differential equations, POD uses basis functions that are generated from numerical solutions of the system or from experimental measurements.

For given $n \in \mathbb{N}$ let

$$0 = t_1 < t_2 < t_2 < \ldots < t_n = T$$

denote an equidistant grid in the interval $[0,T]$ with mesh size $\delta t = t_j - t_{j-1}$, $j = 2,\dots,n$. We assume that δt is a multiple of $\delta\tau$, i.e., $\delta t = \sigma\delta\tau$ with an integer σ. Then $t_j = \tau_{1+\sigma j}$.

Let $\{y_j\}_{j=1}^n \subset \overline{y}^h + V_h$ be the snapshots of the discretized Navier-Stokes equations at given times $\{t_j\}_{j=1}^n$, for example $y_j = y_{1+\sigma j}^h$ with the solutions of the scheme (14). Let

$$V_s = \operatorname{span}\{v_1,\dots,v_n\}, \quad v_i = y_i - \overline{y}^h,$$

have dimension $d \le n$.

One of the central issues of POD is the reduction of data expressing their essential information by means of a few basis vectors. To this end, let W be a Hilbert space with $V_s \subset W$, for example $W = L^2(\Omega)^2$ or $W = H_0^1(\Omega)^2$ and let $\{\phi_i\}_{i=1}^d$ denote an orthonormal basis of V_s with respect to $(\cdot,\cdot)_W$. Then each member of the snapshot ensemble can be expressed as

$$y_j = \overline{y}^h + \sum_{i=1}^{d} (v_j,\phi_i)_W \phi_i, \quad j = 1,..,n.$$

The task of POD is to find an orthonormal basis of size $l \ll n$ such that the mean square error between the snapshots $\{y_j\}_{j=1}^n$ and their representation in the reduced space is minimized on average: For weights $\alpha_j > 0$ consider

$$\begin{aligned} \min_{\{\phi_i\}_{i=1}^l} \quad & \sum_{j=1}^{n} \alpha_j \|v_j - \sum_{i=1}^{l} (v_j,\phi_i)_W \phi_i\|_W^2 \\ \text{subject to} \quad & (\phi_i,\phi_j)_W = \delta_{ij} \qquad \text{for } 1 \le i,j \le l. \end{aligned} \tag{17}$$

The solution $\{\phi_i\}_{i=1}^l$ is called POD basis of rank l. The subspace spanned by the first l POD basis functions is denoted by V_l.

To compute the POD basis, we introduce the correlation matrix $K = (K_{ij}) \in \mathbb{R}^{n\times n}$ corresponding to the snapshots $\{v_j\}_{j=1}^n$ by

$$K_{ij} = \alpha_j (v_j, v_i)_W.$$

The matrix K is positive semi-definite and has rank d.

The solution of (17) can be obtained by solving the symmetric $n \times n$ eigenvalue problem

$$Kx_i = \lambda_i x_i \qquad \text{for } i = 1,\dots,l$$

and setting

$$\phi_i = \frac{1}{\sqrt{\lambda_i}} \sum_{j=1}^{n} \alpha_j (x_i)_j v_j, \qquad i = 1,\dots,l.$$

We have the following error formula

$$\sum_{j=1}^{n} \alpha_j \|v_j - \sum_{i=1}^{l} (v_j,\phi_i)_W \phi_i\|_W^2 = \sum_{i=l+1}^{d} \lambda_i, \tag{18}$$

see [35] for a proof and for more details on the POD basis.

For the application of POD to concrete problems the choice of l is important.

The larger the corresponding eigenvalue λ_i, the more important is the POD basis function ϕ_i for the approximation of the data. In order to obtain a low-dimensional basis for the Galerkin ansatz, modes corresponding to small eigenvalues are neglected.

The minimal number $l \leq n$ of POD basis elements to capture a fraction of $\delta\%$ of the energy in the snapshot set can be determined by selecting the minimal l such that

$$\frac{\sum_{i=1}^{l} \lambda_i}{\sum_{i=1}^{n} \lambda_i} > \delta\%.$$

In fact, as seen in (18), this ratio is the percentage of the total energy captured in the first l POD basis functions and therefore is an index to measure how closely the l-dimensional subspace V_l approximates the snapshot set.

The construction of the reduced order model based on the POD basis elements is discussed in the following section.

5.2. *POD Galerkin approximation*

The idea of POD Galerkin projection is to apply the Galerkin scheme (13) with a low dimensional subspace V_l spanned by POD basis functions instead of V_h, where V_l should approximate the solution trajectory $y(t) - \overline{y}$ sufficiently well. The velocity field in the physical domain Ω is thus approximated by l spatial modes ϕ_i and corresponding time-dependent coefficients β_i.

In the POD Galerkin projection, we thus represent the dynamics of $y(x,t)$ in a given orthonormal basis $\{\phi_j\}_{j=1}^{l} \subset W$ by the approximation

$$y^l(x,t) := \overline{y}(x) + \sum_{j=1}^{l} \beta_j(t)\phi_j(x). \tag{19}$$

Since ϕ_j is an orthonormal basis in W we can recover the time-dependent coefficients by

$$\beta_j(t) := (y^l(\cdot,t) - \overline{y}, \phi_j)_W, \quad j = 1, \ldots, l.$$

In our approach, the basis functions $\{\phi_j\}_{j=1}^{l}$ will be computed by the POD method applied to a well selected set of snapshots $\{y_j - \overline{y}\}_{j=1}^{n}$, where we choose

$$\overline{y} = \frac{1}{n} \sum_{j=1}^{n} y_j.$$

Since the snapshots y_j are divergence free and satisfy the same Dirichlet data y_b, we have $y_j - \overline{y} \in V_h$, $\forall j = 1, \ldots, n$.

The reduced dynamical system is now obtained by inserting (19) into the weak form (9) of the Navier-Stokes system and using $V_l = \operatorname{span}\{\phi_1, \ldots, \phi_l\}$ as test space.

This results in

$$\begin{aligned}(y_0^l - y_0, \phi_j)_{L^2(\Omega)} &= 0,\\ (y_t^l, \phi_j)_{L^2(\Omega)} + \widehat{b}(y^l, y^l, \phi_j) + \nu(\nabla y^l, \nabla\phi_j)_{L^2(\Omega)} &= (f_a + f_c(u), \phi_j)_{L^2(\Omega)}, \qquad (20)\\ &\forall\, j = 1, \ldots, l,\end{aligned}$$

which may be rewritten as

$$\begin{aligned}M\dot{\beta} + n(\beta,\beta) + \nu A\beta &= F(u) + r,\\ \beta(0) &= ((y_0 - \overline{y}, \phi_j)_W)_{j=1}^l.\end{aligned}$$

$M = ((\phi_i, \phi_j)_{L^2(\Omega)})_{i,j=1}^l$ denotes the POD mass matrix, $A = ((\nabla\phi_i, \nabla\phi_j)_{L^2(\Omega)})_{i,j=1}^l$ the POD stiffness matrix, $n(\beta,\beta)$ the convection term, $F(u) = ((f_c(u), \phi_j)_{L^2(\Omega)})_{j=1}^l$ and r results from the contribution of the mean $\overline{y}$ and f_a.

Remark 1 Pressure neglection. In view of our application to the Navier-Stokes equations let us note that the POD basis elements inherit the boundary and incompressibility conditions of the snapshots. The Galerkin projection on divergence-free modes and subsequent integration by parts reduces the pressure term to a boundary integral that vanishes.

Remark 2 Efficient evaluation of the nonlinearity.

The convection term leads to the nonlinearity $\widehat{b}(y^l, y^l, \phi_j)$. A common problem in the standard POD-Galerkin technique is that the complexity for the evaluation of the nonlinear term remains that of the original problem. There are new approaches using Discrete Empirical Interpolation (DEIM) to overcome the deficiencies of POD with respect to nonlinearties, see e.g. [8, 9].

Due to the bilinearity of the nonlinear convection term of the Navier-Stokes equations, the term can be splitted as follows. Let $\Phi = [\phi_1, \ldots, \phi_l]$ and denote by $\widehat{b}\left(y^l, y^l, \Phi\right)$ the column vector $(\widehat{b}\left(y^l, y^l, \phi_i\right))_{i=1}^l$ and by $\widehat{b}\left(y^l, \Phi, \Phi\right)$ the matrix $(\widehat{b}\left(y^l, \phi_j, \phi_i\right))_{i,j=1}^l$. Then

$$\begin{aligned}\widehat{b}\left(y^l, y^l, \Phi\right) &= \widehat{b}\left(y^l, \overline{y}, \Phi\right) + \sum_{j=1}^{l} \widehat{b}\left(y^l, \phi_j, \Phi\right)\beta_j\\ &= \widehat{b}\left(y^l, \overline{y}, \Phi\right) + \widehat{b}\left(y^l, \Phi, \Phi\right)\beta\\ &= \widehat{b}\left(\overline{y}, \overline{y}, \Phi\right) + \sum_{i=1}^{l}\beta_i b\left(\phi_i, \overline{y}, \Phi\right) + \left[b\left(\overline{y}, \Phi, \Phi\right) + \sum_{i=1}^{l}\beta_i b\left(\phi_i, \Phi, \Phi\right)\right]\beta\\ &=: n(\beta,\beta).\end{aligned}$$

The vectors $\widehat{b}\left(\overline{y}, \overline{y}, \Phi\right), \widehat{b}\left(\phi_i, \overline{y}, \Phi\right)$ and the matrices $\widehat{b}\left(\overline{y}, \Phi, \Phi\right), \widehat{b}\left(\phi_i, \Phi, \Phi\right)$ for $i = 1, \ldots, l$ can be calculated offline for the POD basis elements. Online these terms can be combined by linear combination with the coefficients $\beta = (\beta_1, \ldots, \beta_l)^T$. Thus, the calculation of the nonlinearity can be executed in the reduced dimension and the performance for calculating the nonlinear convection term can significantly be increased.

The reduced optimization problem corresponding to (7) is obtained by inserting (19) into the cost functional and utilizing the reduced dynamical system as

constraint in the optimization process:

$$\begin{aligned} & \min \quad J_T(\beta, u) \\ \text{subject to} \quad & M\dot{\beta} + \nu A\beta + n(\beta, \beta) = F(u) + r \\ & \beta(0) = \beta_0. \end{aligned} \tag{21}$$

5.3. *Snapshot Generation*

The important question in constructing a POD basis for a specific problem is the choice of the snapshot ensemble. The effectiveness of the POD basis resides in the generation of a good snapshot basis, which is capable of capturing the dynamics of the flow.

In model reduction for simulation purposes, the basis functions are obtained for a given configuration or parameter regime. The complete flow information is then already contained in the snapshot ensemble and so the reduced model yields a good approximation of the original solution. Moreover, in this case, the POD basis needs a small number of basis elements and can still obtain a satisfactory level of accuracy.

Model reduction for control is more challenging. The basis functions might be sufficient to reproduce the dynamics of the flow for a fixed system, but not suitable for other simulations. That is exactly the case when a control is acting on the flow.

In literature there are different approaches how to choose the snapshots for a ROM under control:

One approach is to enlarge the computational database in order to include the effect of controls. In [32] the flow is simulated under the action of a random control to enrich the snapshot ensemble. We have applied a version of this approach to our setting, combining snapshots of the uncontrolled flow and of the flow under the action of one control parameter setting. Unfortunately, this did not lead to any cancellation results. Adding more snapshots for more control settings would have increased the POD basis so much that the reduced dimension would have been far too large.

In [28] and [1] adaptive procedures are developed that improve the ROM by successively updating the ensemble of data. It is tested on a recirculation control problem in channel flow [28] and the wake flow around a cylinder [1] and works quite effectively. In each iteration of this adaptive procedure the optimized control is used to compute new snapshots, which are used to create a new POD subspace. The reduced-order control system is solved with the new subspace to find a new optimal control. After each optimization step a Finite Element simulation has to be carried out to obtain the new snapshots. This procedure is not applicable in our setting, where we aim for real-time control and cannot execute a time-consuming Finite Element simulation.

Diwoky and Volkwein obtain an efficient reduced-order method for a boundary control problem of the heat equation by including information of the state as well as of the adjoint into the POD basis, see [12]. In order to generate these adjoint snapshots, this approach requires an adjoint solver of the dynamical system, which might be not available for every simulation. Considering the generation of snapshots by experimental measurements, the generation of adjoint snapshots is not possible, so that the snapshot ensemble should work without the additional information.

An idea to characterize the input-output behavior of the actuation in a better way and to enrich the snapshots with this information are impulse response snap-

shots. In [24] impulse response snapshots are used to describe the actuation effect. Snapshot-based balanced truncation, also known as BPOD, takes into account controllability and observability [30]. The most controllable modes are found with data from the response of the state of the system to an impulse input.

5.3.1. Impulse Response Snapshots

In order to characterize the input-output behavior of the actuation, snapshots have to be found that allow to infer how the system will respond to inputs which have not been measured. By taking into account linear systems, it is possible to use the responses to a small set of inputs to predict the response to any possible input. This can save an enormous amount of work, and enables the complete characterization of the system.

We write the Navier-Stokes equation $E(y - \overline{y}, u) = 0$ according to (10) in the form

$$C(y) = f_a + f_c(u), \qquad y(0) = y_0 \tag{22}$$

and linearize the Navier-Stokes system around the steady state solution y_s

$$C(y_s) = 0, \qquad y_s(0) = y_s.$$

By the differentiability of the Navier-Stokes operator (10) the linearized Navier-Stokes equation satisfies

$$C(y) = C_y(y_s)(y - y_s) + O(\|y - y_s\|_Y^2), \tag{23}$$

and hence y satisfies, up to an error of $O(\|y - y_s\|_Y^2)$, the linearized equation

$$\begin{aligned} C_y(y_s)(\tilde{y} - y_s) &= f_a + f_c(u), \\ \tilde{y}(0) - y_0 &= 0. \end{aligned} \tag{24}$$

Now let y_a be the unique solution of

$$C_y(y_s)(y_a - y_s) = f_a, \quad y_a(0) = y_0,$$

then the linearized equation (24) can be rewritten as

$$\begin{aligned} C_y(y_s)(\tilde{y} - y_a) &= f_c(u), \\ \tilde{y}(0) - y_a(0) &= 0. \end{aligned} \tag{25}$$

We recall that $f_c(u; x, t) = u(t)g(x)$. Therefore, the solution of (25) can be represented by means of the impulse response w corresponding to g. To this end we formulate the impulse response equation by

$$\begin{aligned} C_y(y_s)w &= 0, \\ (w(0) - g, \phi)_{L^2(\Omega)} &= 0 \quad \forall\, \phi \in V. \end{aligned} \tag{26}$$

Using convolution, the output of the system (24) can be constructed for any input signal u, if the impulse response w is known:

$$\tilde{y}(t) = y_a(t) + \int_0^t u(s)w(t - s)\ \mathrm{ds}\ .$$

This shows that $\tilde{y}(t) \in y_a(t)+\text{span}\{w(s) \,:\, s \in [0,t]\}$ and $y(t)$ satisfies the inclusion up to an error of order $O(\|y - y_s\|_Y^2)$. This motivates to build a POD basis based on snapshots of y_a and w. By iterating the process (simplified Newton method), a subspace V_l can be identified such that the order of the error can be increased.

An analogous approach can be applied to the scheme (14) instead of the PDE (10), where the convolution formula has to be replaced by a discrete analogue. We will discuss and analyze this approach in detail in 6.3.

In order to avoid the usage of the linearized equation, e.g. if the snapshots shall be generated by experimental measurements of flow fields, we can also work with the nonlinear PDE (22). Another advantage is that the nonlinear snapshots contain more specific information of the underlying dynamical system. More precise, we choose y_a as the solution of (22) for $u = 0$ and the impulse response system (26) equals approximately

$$\begin{aligned} C(\epsilon w + y_s) &= 0, \\ (w(0) - g, \phi)_{L^2(\Omega)} &= 0 \quad \forall\, \phi \in V, \end{aligned}$$

which can be seen by choosing $y = \epsilon w + y_s$ in (23). Note that ϵ has to be chosen appropriately, such that ϵg is a sufficiently small variation of y_s.

6. A-Priori Error Estimates

We want to give an error estimate for the error

$$\|(y_k^l - y(\tau_k))\|^2_{L^2(I,H_0^1)} = \sum_{k=1}^{m} \delta\tau \|y_k^l - y(\tau_k)\|^2_{H_0^1}$$

between the reduced order model and the exact solution of the Navier-Stokes equations.

We can split this in three terms:

$$\begin{aligned} \|(y_k^l - y(\tau_k))\|^2_{L^2(I,H_0^1)} \le\ & 3\|(y_k^l - y_k^h)\|^2_{L^2(I,H_0^1)} \\ & + 3\|(y_k^h - y^h(\tau_k))\|^2_{L^2(I,H_0^1)} + 3\|(y^h(\tau_k) - y(\tau_k))\|^2_{L^2(I,H_0^1)}. \end{aligned} \quad (27)$$

Let $y(\tau_k) \in \overline{y} + W(I)$ be the solution of the Navier-Stokes system (9) and

$$y^h(\tau_k) = \overline{y}^h + v^h(\tau_k) \in \overline{y}^h + V_h$$

be the solution of the semi-discrete FE system (13) at the time instances $t = \tau_k$, $k = 1, \dots, m$. The solution of the discretized FE system (14) and the discretized ROM system (20) is denoted by

$$y_k^h = \overline{y}^h + v_k^h \in \overline{y}^h + V_h,$$

$$y_k^l = \overline{y}^h + \sum_{j=1}^{l} \beta_j(\tau_k)\phi_j(x) = \overline{y}^h + v_k^l \in \overline{y}^h + V_l,$$

respectively.

For simplicity, we assume in this section, that the two time increments coincide, i.e., $\tau_i = t_i$ for $i = 1, \ldots, m$ and $n = m$.

An estimate for the first term is given in the next section 6.1.

6.1. *Error between ROM and Finite Element method*

Our next goal is to derive an error estimate for the error

$$\|(y_k^l - y_k^h)\|^2_{L^2(I,H_0^1)} = \sum_{k=1}^{m} \delta\tau \|y_k^l - y_k^h\|^2_{H_0^1}$$

between the reduced order model and the discrete Finite Element solution.

We will adapt and extend the arguments by Kunisch and Volkwein in [23] for backward Euler time discretization. In [22] one can find an error estimate for the Crank-Nicolson time discretization.

We are using the same decomposition as [23]

$$y_k^l - y_k^h = v_k^l - v_k^h = \underbrace{v_k^l - P^l v_k^h}_{\vartheta_k} + \underbrace{P^l v_k^h - v_k^h}_{\varrho_k}.$$

with the projection $P^l : V_h \to V_l$.

The estimate for ϑ_k – the error between the reduced order model and the projection of the discrete Finite Element solution – can be found in the next section 6.2.

An estimate for ϱ_k – the error between the projection of the discrete Finite Element solution and the discretized Finite Element solution – is derived in section 6.3.

6.2. *Error between ROM and Finite Element projection*

We obtain the following error estimate for ϑ_k.

LEMMA 6.1 *There exists a constant $C_\vartheta > 0$ independent of h and of the grids $\{t_j\}_{j=0}^n$ and $\{\tau_j\}_{j=0}^m$ such that*

$$\begin{aligned} \|(\vartheta_k)\|^2_{L^2(I,H_0^1)} \le C_\vartheta \Big(& \|\vartheta_0\|^2_{L^2} + \delta\tau\nu \|\vartheta_0\|^2_{H_0^1} \\ & + \|(\overline{\partial}_\tau y_k^h - \overline{\partial}_\tau P^l y_k^h)\|^2_{L^2(I,H_0^1)} + 2\|(\varrho_k)\|^2_{L^2(I,H_0^1)} \Big) \end{aligned} \tag{28}$$

Proof The proof follows the one of Lemma 4.5 in [23] except of the following changes due to the different time discretization and we obtain directly an estimate in $L^2(I, H_0^1)$.

We introduce the bilinear operator B satisfying

$$\Big\langle B(v^h, w^h), \phi^h \Big\rangle_{H^{-1},H_0^1} := \widehat{b}(v^h, w^h, \phi^h)$$

for all $v^h, w^h, \phi^h \in V_h$.

y_k^l satisfying (20) and y_k^h satisfying (14), we obtain

$$\begin{aligned}(\overline{\partial}\vartheta_k, \phi^h)_{L^2} + \nu(\nabla\vartheta_k, \nabla\phi^h) \\ = (z_k, \phi^h)_{L^2} + \left\langle B(v_{k-1}^h, v_k^h) - B(v_{k-1}^l, v_k^l), \phi^h \right\rangle_{H^{-1},H_0^1} \\ + \left\langle B(\overline{y}^h, v_k^h - v_k^l) + B(v_{k-1}^h - v_{k-1}^l, \overline{y}^h), \phi^h \right\rangle_{H^{-1},H_0^1} \end{aligned} \tag{29}$$

for all $\phi^h \in V_l$, where

$$z_k = \overline{\partial}_\tau v_k^h - \overline{\partial}_\tau P^l v_k^h.$$

Choosing $\phi^h = \vartheta_k \in V_l$, we infer that

$$\begin{aligned}\|\vartheta_k\|_{L^2}^2 - \|\vartheta_{k-1}\|_{L^2}^2 + \|\vartheta_k - \vartheta_{k-1}\|_{L^2}^2 + 2\delta\tau\nu\|\vartheta_k\|_{H_0^1}^2 \\ \le 2\delta\tau \left(\|z_k\|_{L^2}\|\vartheta_k\|_{L^2} + \left| \left\langle B\left(v_{k-1}^h, v_k^h\right) - B\left(v_{k-1}^l, v_k^l\right), \vartheta_k \right\rangle_{H^{-1},H_0^1} \right| \right. \\ \left. + \left| \left\langle B(\overline{y}^h, v_k^h - v_k^l) + B(v_{k-1}^h - v_{k-1}^l, \overline{y}^h), \vartheta_k \right\rangle_{H^{-1},H_0^1} \right| \right). \end{aligned} \tag{30}$$

The nonlinear terms on the right-hand side of (30) can be splitted into

$$\begin{aligned}B(v_{k-1}^h, v_k^h) - B(v_{k-1}^l, v_k^l) = &- B(v_{k-1}^l - v_{k-1}^h, v_k^h) \\ &- B(v_{k-1}^l - v_{k-1}^h, v_k^l - v_k^h) \\ &- B(v_{k-1}^h, v_k^l - v_k^h).\end{aligned}$$

The terms can be estimated as follows:

$$\left| \left\langle B\left(v_{k-1}^h, v_k^l - v_k^h\right), \vartheta_k \right\rangle_{H^{-1},H_0^1} \right| \le \frac{\nu}{10}\|\vartheta_k\|_{H_0^1}^2 + c_1\|\vartheta_k\|_{L^2}^2 + c_2\|\varrho_k\|_{H_0^1}^2,$$

$$\begin{aligned}&\left| \left\langle B\left(v_{k-1}^l - v_{k-1}^h, v_k^h\right), \vartheta_k \right\rangle_{H^{-1},H_0^1} \right| \\ &\quad \le \frac{\nu}{10}\|\vartheta_k\|_{H_0^1}^2 + c_3\|\vartheta_k\|_{L^2}^2 + c_4\|\varrho_{k-1}\|_{H_0^1}^2 + c_5\|\vartheta_{k-1}\|_{L^2}^2 + \frac{\nu}{12}\|\vartheta_{k-1}\|_{H_0^1}^2, \end{aligned} \tag{31}$$

$$\begin{aligned}&\left| \left\langle B\left(v_{k-1}^l - v_{k-1}^h, v_k^l - v_k^h\right), \vartheta_k \right\rangle_{H^{-1},H_0^1} \right| \\ &\qquad \le \frac{\nu}{10}\|\vartheta_k\|_{H_0^1}^2 + c_6\|\vartheta_k\|_{L^2}^2 + c_7\|\varrho_k\|_{H_0^1}^2 + c_8\|\vartheta_{k-1}\|_{L^2}^2 + \frac{\nu}{12}\|\vartheta_{k-1}\|_{H_0^1}^2 \end{aligned}$$

and similarly

$$\left| \left\langle B\left(\overline{y}^h, v_k^h - v_k^l\right), \vartheta_k \right\rangle_{H^{-1},H_0^1} \right| \le \frac{\nu}{10}\|\vartheta_k\|_{H_0^1}^2 + c_9\|\vartheta_k\|_{L^2}^2 + c_{10}\|\varrho_k\|_{H_0^1}^2,$$

$$\left|\left\langle B\left(v_{k-1}^h - v_{k-1}^l, \overline{y}^h\right), \vartheta_k\right\rangle_{H^{-1},H_0^1}\right|$$
$$\leq \frac{\nu}{10}\|\vartheta_k\|_{H_0^1}^2 + c_{11}\|\vartheta_k\|_{L^2}^2 + c_{12}\|\varrho_{k-1}\|_{H_0^1}^2 + c_{13}\|\vartheta_{k-1}\|_{L^2}^2 + \frac{\nu}{12}\|\vartheta_{k-1}\|_{H_0^1}^2.$$

Combining the estimates, we obtain

$$\begin{aligned}\|\vartheta_k\|_{L^2}^2 + \delta\tau\nu\|\vartheta_k\|_{H_0^1}^2 \leq &(1+\delta\tau c_{14})\|\vartheta_{k-1}\|_{L^2}^2 + \delta\tau\frac{\nu}{2}\|\vartheta_{k-1}\|_{H_0^1}^2 \\ &+ \delta\tau\left(c_{15}\|\vartheta_k\|_{L^2}^2 + \|z_k\|_{L^2}^2 + c_{16}\|\varrho_k\|_{H_0^1}^2 + c_{17}\|\varrho_{k-1}\|_{H_0^1}^2\right)\end{aligned}$$

where $c_{14} = c_5 + c_8 + c_{13}$, $c_{15} = 1 + c_1 + c_3 + c_6 + c_9 + c_{11}$, $c_{16} = c_2 + c_7 + c_{10}$, $c_{17} = c_4 + c_{12}$.

By adding on each side the sum $\sum_{j=1}^{k-1}\delta\tau\frac{\nu}{2}\|\vartheta_j\|_{H_0^1}^2$ we obtain

$$\begin{aligned}&\underbrace{\|\vartheta_k\|_{L^2}^2 + \delta\tau\frac{\nu}{2}\|\vartheta_k\|_{H_0^1}^2 + \sum_{j=1}^{k}\delta\tau\frac{\nu}{2}\|\vartheta_j\|_{H_0^1}^2}_{\omega_k} \\ &\quad\leq (1+\delta\tau c_{14})\underbrace{\left(\|\vartheta_{k-1}\|_{L^2}^2 + \delta\tau\frac{\nu}{2}\|\vartheta_{k-1}\|_{H_0^1}^2 + \sum_{j=1}^{k-1}\delta\tau\frac{\nu}{2}\|\vartheta_j\|_{H_0^1}^2\right)}_{\omega_{k-1}} \\ &\quad\quad+\delta\tau\left(c_{15}\underbrace{\left(\|\vartheta_k\|_{L^2}^2 + \delta\tau\frac{\nu}{2}\|\vartheta_k\|_{H_0^1}^2 + \sum_{j=1}^{k}\delta\tau\frac{\nu}{2}\|\vartheta_j\|_{H_0^1}^2\right)}_{\omega_k}\right) \\ &\quad\quad+\delta\tau\left(\|z_k\|_{L^2}^2 + c_{16}\|\varrho_k\|_{H_0^1}^2 + c_{17}\|\varrho_{k-1}\|_{H_0^1}^2\right). \quad (32)\end{aligned}$$

Suppose that

$$\delta\tau \leq \frac{1}{2c_{15}}. \quad (33)$$

With (33) holding, we have $1 - c_{15}\delta\tau \geq \frac{1}{2}$ and

$$\frac{1+c_{14}\delta\tau}{1-c_{15}\delta\tau} = 1 + \frac{(c_{14}+c_{15})\delta\tau}{1-c_{15}\delta\tau} \leq 1 + 2(c_{14}+c_{15})\delta\tau. \quad (34)$$

From (32) and (34) we find that

$$\begin{aligned}\omega_k \leq &(1+2(c_{14}+c_{15})\delta\tau) \\ &\cdot\left(\omega_{k-1} + \delta\tau\left(\|z_k\|_{L^2}^2 + c_{16}\|\varrho_k\|_{H_0^1}^2 + c_{17}\|\varrho_{k-1}\|_{H_0^1}^2\right)\right)\end{aligned}$$

holds. By summation over k we obtain

$$\begin{aligned}\omega_k \leq & \left(1+\frac{2(c_{14}+c_{15})\delta\tau}{\delta\tau}\frac{k\delta\tau}{k}\right)^k \\ & \cdot\left(\omega_0+\sum_{j=1}^{k}\delta\tau\left(\|z_j\|_{L^2}^2+c_{16}\|\varrho_j\|_{H_0^1}^2+c_{17}\|\varrho_{j-1}\|_{H_0^1}^2\right)\right) \\ \leq & e^{c_{18}k\delta\tau}\left(\omega_0+\sum_{j=1}^{k}\delta\tau\left(\|z_j\|_{L^2}^2+c_{16}\|\varrho_j\|_{H_0^1}^2+c_{17}\|\varrho_{j-1}\|_{H_0^1}^2\right)\right) \end{aligned} \tag{35}$$

where $c_{18}=2(c_{14}+c_{15})$.

There exist a constant C such that

$$\|(\vartheta_k)\|_{L^2(I,H_0^1)}^2 \leq C\left(\|\vartheta_0\|_{L^2}^2+\delta\tau\nu\|\vartheta_0\|_{H_0^1}^2+\|(z_k)\|_{L^2(I,H_0^1)}^2+2\|(\varrho_k)\|_{L^2(I,H_0^1)}^2\right)$$

the claim follows. ■

Now, we have to estimate $\|(\varrho_k)\|_{L^2(I,H_0^1)}^2$ and $\|(z_k)\|_{L^2(I,H_0^1)}^2$.

6.3. *Error estimate for impulse response snapshots*

We estimate

$$\|(\varrho_k)\|_{L^2(I,H_0^1)}^2 = \|(P^l v_k^h - v_k^h)\|_{L^2(I,H_0^1)}^2$$

for the particular reduced order model proposed in this paper.

As outlined in 5.3.1 we generate snapshots of the impulse response w given by (26). We consider the case, where the impulse response is generated by the semi-implicit Euler Galerkin scheme (14). Using the notations of (14) and (15) we have

$$\left\langle C^{h,k}(y_k^h,y_{k-1}^h),\phi^h\right\rangle_{V_h',V_h} = (\overline{\partial}_\tau y_k^h,\phi^h)_{L^2(\Omega)}+\widehat{b}(y_{k-1}^h,y_k^h,\phi^h)+\nu(\nabla y_k^h,\nabla\phi^h)_{L^2(\Omega)}$$

and the semi-implicit Euler Galerkin scheme (14) reads: Find $y_k^h \in \overline{y}^h+V_h$ with

$$\begin{aligned}\left\langle C^{h,k}(y_k^h,y_{k-1}^h)-f_a-f_c(u_k),\phi^h\right\rangle_{V_h',V_h} &= 0 \quad \forall\,\phi^h\in V_h,\quad k=1,\dots,m,\\ (y_0^h-y_0,\phi^h)_{L^2(\Omega)} &= 0 \quad \forall\,\phi^h\in V_h.\end{aligned} \tag{36}$$

Let $y_s^h \in \overline{y}^h+V_h$ be the discrete steady state, i.e.,

$$\left\langle C^{h,k}(y_s^h,y_s^h),\phi^h\right\rangle_{V_h',V_h} = 0 \quad \forall\,\phi^h\in V_h,\quad k=1,\dots,m.$$

Then the discrete version of the linearized state equation (24) is

$$\begin{aligned}\Big\langle C^{h,k}_{y_k}(y^h_s,y^h_s)(\tilde y^h_k - y^h_s) + C^{h,k}_{y_{k-1}}(y^h_s,y^h_s)(\tilde y^h_{k-1} - y^h_s) \\ -f_a - f_c(u_k), \phi^h\Big\rangle_{V_h',V_h} = 0 \quad \forall\, \phi^h \in V_h,\ k = 1,\dots,m, \\ (\tilde y^h_0 - y_0, \phi^h)_{L^2(\Omega)} = 0 \quad \forall\, \phi^h \in V_h.\end{aligned} \tag{37}$$

Here, we have used that $f_c(u)$ in (2) depends linearly on u.

We now proceed as outlined in 5.3.1. Let $y^h_{a,k}$ be a solution of (37) for $u_k = 0$. The discrete approximation of the impulse response problem (26) is given by

$$\begin{aligned}\Big\langle C^{h,k}_{y_k}(y^h_s,y^h_s)w^h_k + C^{h,k}_{y_{k-1}}(y^h_s,y^h_s)w^h_{k-1}, \phi^h\Big\rangle_{V_h',V_h} = 0 \quad \forall\, \phi^h \in V_h,\quad k = 1,\dots,m, \\ (\tilde y^h_0 - g, \phi^h)_{L^2(\Omega)} = 0 \quad \forall\, \phi^h \in V_h.\end{aligned}$$

For $k \geq 1$ this coincides with the solution for initial data $w^h_0 = 0$ and right hand side $f_c(\delta_{1k}/\delta\tau)$ with the Kronecker symbol δ_{ij}. Therefore, it is easy to see that the solution of (37) can be obtained by the discrete convolution formula

$$\tilde y^h_k = y^h_{a,k} + \sum_{j=0}^{k-1} \delta\tau\, u_{j+1}\, w^h_{k-j}. \tag{38}$$

Hence, all solutions of (37) satisfy

$$\tilde y^h_k \in y^h_{a,k} + \operatorname{span}\{w^h_1,\dots,w^h_k\}.$$

6.3.1. Snapshot selection and POD basis

We consider the following construction of the POD basis. For

$$s^h_i = y^h_{a,i} - y^h_s, \quad i = 0,\dots,n, \qquad s^h_{m+i} = w^h_i, \quad i = 1,\dots,n,$$

we choose the snapshot set

$$W_h = \operatorname{span}\{s^h_0,\dots,s^h_{2n+1}\} \tag{39}$$

with dimension $d \leq 2n+1$ and denote by $\{\phi_1,\dots,\phi_d\}$ the corresponding POD basis with respect to the H^1_0 scalar product for the weights $\alpha_j = \delta\tau$ in (17).

Moreover, set $V_l := \operatorname{span}\{\phi_1,\dots,\phi_l, y^h_s - \overline{y}^h\}$, $l \leq d$, let $P^l : H^1_0 \mapsto V_l$ be the orthogonal projection in H^1_0. Finally, let λ_i be the eigenvalues of the correlation matrix $K = (\delta\tau(s^h_i, s^h_j)_{H^1_0})_{1\leq i,j\leq 2n+1}$.

6.3.2. Approximation property

We have the following approximation result.

LEMMA 6.2 *Let W_h, V_l, P^l and λ_i be as in section 6.3.1. Then for any solution of (37) one has*

$$\begin{aligned}\|\tilde{y}_k^h - y_{a,k}^h - P^l(\tilde{y}_k^h - y_{a,k}^h)\|_{H_0^1}^2 &\le \|(u_j)\|_{L^2(I;\mathbb{R})}^2 \|w_j^h - P^l(w_j^h)\|_{L^2(I;H_0^1)}^2 \\ &\le \|(u_j)\|_{L^2(I;\mathbb{R})}^2 \sum_{i=l+1}^{d} \lambda_i,\end{aligned}$$

$$\|(y_{a,k}^h - \overline{y}^h - P^l(y_{a,k}^h - \overline{y}^h))\|_{L^2(I;H_0^1)}^2 \le \sum_{i=l+1}^{d} \lambda_i.$$

Proof (38) and (18) yield

$$\|\tilde{y}_k^h - y_{a,k}^h - P^l(\tilde{y}_k^h - y_{a,k}^h)\|_{H_0^1}^2 = \left\| \sum_{j=0}^{k-1} \delta\tau u_{j+1}(w_{k-j}^h - P^l w_{k-j}^h) \right\|_{H_0^1}^2$$

$$\le \left(\sum_{j=1}^{m} \delta\tau |u_j|^2 \right) \left(\sum_{j=1}^{m} \delta\tau \|w_j^h - P^l w_j^h\|_{H_0^1}^2 \right) \le \|(u_j)\|_{L^2(I;\mathbb{R})}^2 \sum_{i=l+1}^{d} \lambda_i.$$

Since $y_s^h - \overline{y}^h \in V_l$, we have $y_{a,k}^h - \overline{y}^h - P^l(y_{a,k}^h - \overline{y}^h) = y_{a,k}^h - y_s^h - P^l(y_{a,k}^h - y_s^h)$. The estimate for $\|y_{a,k}^h - y_s^h - P^l(y_{a,k}^h - y_s^h)\|_{L^2(I;H_0^1)}^2$ follows directly from (18) and the fact that $y_{a,k}^h - y_s^h$ is contained in the snapshot set W_h. ∎

We now estimate the error

$$\|(\varrho_k)\|_{L^2(I;H_0^1)} = \|(v_k^h - P^l v_k^h)\|_{L^2(I;H_0^1)} = \|(y_k^h - \overline{y}^h - P^l(y_k^h - \overline{y}^h))\|_{L^2(I;H_0^1)}$$

for solutions of the nonlinear scheme (36).

LEMMA 6.3 *Let as above $v_k^h := y_k^h - \overline{y}^h$. Then we have the estimate*

$$\begin{aligned}\|(v_k^h - P^l v_k^h))\|_{L^2(I;H_0^1)}^2 \le C \left(\|(y_k^h - y_s^h)\|_{L^4(I;H_0^1)}^4 + \|(y_{k-1}^h - y_s^h)\|_{L^4(I;H_0^1)}^4 \right) \\ + 2(T\,\|(u_k)\|_{L^2(I;\mathbb{R})}^2 + 1) \sum_{i=l+1}^{d} \lambda_i.\end{aligned}$$

Proof We have $\|(v_k^h - P^l v_k^h))\|_{L^2(I;H_0^1)} = \|(y_k^h - \overline{y}^h - P^l(y_k^h - \overline{y}^h))\|_{L^2(I;H_0^1)}$.

Let y_k^h and $\tilde{y}_k^h$ be the solutions of (36) and (37), respectively. Since P^l is the projection in H_0^1 onto V_l, we have

$$\begin{aligned}\|y_k^h - \overline{y}^h - P^l(y_k^h - \overline{y}^h)\|_{H_0^1} &\le \|y_k^h - \overline{y}^h - (\tilde{y}_k^h - \overline{y}^h)\|_{H_0^1} + \|\tilde{y}_k^h - \overline{y}^h - P^l(\tilde{y}_k^h - \overline{y}^h)\|_{H_0^1} \\ &= \|y_k^h - \tilde{y}_k^h\|_{H_0^1} + \|\tilde{y}_k^h - \overline{y}^h - P^l(\tilde{y}_k^h - \overline{y}^h)\|_{H_0^1}.\end{aligned}$$

By Lemma 6.2 the second term can be estimated by

$$\|(\tilde{y}_k^h - \overline{y}^h - P^l(\tilde{y}_k^h - \overline{y}^h))\|_{L^2(I;H_0^1)}^2 \le (T\,\|(u_k)\|_{L^2(I;\mathbb{R})}^2 + 1) \sum_{i=l+1}^{d} \lambda_i.$$

Now set

$$e_k^h := y_k^h - \tilde{y}_k^h, \quad r_k^h := y_k^h - y_s^h.$$

Since (37) is the linearization of (36) and the nonlinearity in (36) is quadratic, the error $e_k^h := y_k^h - \tilde{y}_k^h$ satisfies for all $\phi^h \in V_h$, $k = 1, \dots, m$,

$$\left\langle C_{y_k}^{h,k}(y_s^h, y_s^h)e_k^h + C_{y_{k-1}}^{h,k}(y_s^h, y_s^h)e_{k-1}^h + \frac{1}{2}C_{y_{k-1}y_k}^{h,k}(y_s^h, y_s^h)[r_{k-1}^h, r_k^h], \phi^h \right\rangle_{V_h', V_h} = 0$$

$$(\tilde{e}_0^h, \phi^h)_{L^2(\Omega)} = 0,$$

which corresponds to the scheme

$$(\overline{\partial}_\tau e_k^h, \phi^h) + \nu(\nabla e_k^h, \nabla \phi^h) + \left\langle (B(e_{k-1}^h, y_s^h) + B(y_s^h, e_k^h), \phi \right\rangle = -\left\langle B(r_{k-1}^h, r_k^h), \phi^h \right\rangle.$$

Now we use the stability of the linearized scheme. Choosing $\phi^h = e_k^h$ yields, similar to (30) and by using $\langle B(y_s^h, e_k^h), e_k^h \rangle = 0$,

$$\begin{aligned} \|e_k^h\|_{L^2}^2 - \|e_{k-1}^h\|_{L^2}^2 + \|e_k^h - e_{k-1}^h\|_{L^2}^2 + 2\delta\tau\nu\|e_k^h\|_{H_0^1}^2 \\ \leq 2\delta\tau \left| \left\langle B(e_{k-1}^h, y_s^h) + B(r_{k-1}^h, r_k^h), e_k^h \right\rangle \right|. \end{aligned} \tag{40}$$

By (8) and (12) the first term on the right hand side can be estimated similarly to (31) by

$$\left| \left\langle (B(e_{k-1}^h, y_s^h), e_k^h \right\rangle \right| \leq \frac{\nu}{4}\|e_k^h\|_{H_0^1}^2 + \frac{\nu}{4}\|e_{k-1}^h\|_{H_0^1}^2 + c(\|y_s^h\|_{H_0^1}) \left(\|e_{k-1}^h\|_{L^2}^2 + \|e_k^h\|_{L^2}^2 \right)$$

and the second by

$$\left| \left\langle B(r_{k-1}^h, r_k^h), e_k^h \right\rangle \right| \leq \frac{\nu}{4}\|e_k^h\|_{H_0^1}^2 + c_1 \left(\|r_{k-1}^h\|_{L^2}^{1/2} \|r_{k-1}^h\|_{H_0^1}^{1/2} \|r_k^h\|_{H_0^1} \right)^2.$$

We conclude that

$$\begin{aligned} \|e_k^h\|_{L^2}^2 + \|e_k^h - e_{k-1}^h\|_{L^2}^2 + \delta\tau\nu\|e_k^h\|_{H_0^1}^2 \leq (1 + c_2\delta\tau)\|e_{k-1}^h\|_{L^2}^2 + \delta\tau\frac{\nu}{2}\|e_{k-1}^h\|_{H_0^1}^2 \\ + \delta\tau \left(c_3\|e_k^h\|_{L^2}^2 + c_4\|r_{k-1}^h\|_{H_0^1}^2 \|r_k^h\|_{H_0^1}^2 \right) \end{aligned}$$

and an application of Gronwall's lemma yields as for (30)

$$\begin{aligned} \|(e_k^h)\|_{L^\infty(I;L^2)}^2 + \frac{\nu}{2}\|(e_k^h)\|_{L^2(I;H_0^1)}^2 + \|(e_k^h - e_{k-1}^h)\|_{L^\infty(I;L^2)}^2 \\ \leq C\left(\|(r_k^h)\|_{L^4(I;H_0^1)}^4 + \|(r_{k-1}^h)\|_{L^4(I;H_0^1)}^4 \right). \end{aligned} \tag{41}$$

■

6.4. *Error between ROM and Navier-Stokes equations*

Finally, we obtain the following theorem.

THEOREM 6.4 *There exist constants C_1, C_2 and $c(\|u\|_{L^2})$ independent of h and the grid, such that*

$$\begin{aligned}\|(y_k^l - y(\tau_k))\|^2_{L^2(I,H_0^1)} \le C_1 \Bigg[& \|v_0^l - P^l v^h(\tau_0)\|^2_{L^2} + \delta\tau\nu \|v_0^l - P^l v^h(\tau_0)\|^2_{H_0^1} \\ & + (\frac{1}{\delta\tau^2} + 1) \left(\|(y_k^h - y_s^h)\|^4_{L^4(I;H_0^1)} + \|(y_{k-1}^h - y_s^h)\|^4_{L^4(I;H_0^1)} \right) \\ & + (\frac{1}{\delta\tau^2} + 1)(T\,\|(u_k)\|^2_{L^2(I;\mathbb{R})} + 1) \sum_{i=l+1}^{d} \lambda_i \Bigg] \\ & + C_2 \delta\tau^2 \|y_{tt}^h\|^2_{L^2(I,H_0^1)} + c(\|u\|_{L^2}) \left(h + \inf_{\phi_h \in V_h} \|\overline{y} - \overline{y}^h - \phi^h\| \right).\end{aligned}$$

Proof We can combine now the estimates for each term in (27). The first term is estimated by Lemma 6.1, Lemma 6.3 and

$$\begin{aligned}\|(\overline{\partial}_\tau y_k^h - \overline{\partial}_\tau P^l y_k^h)\|^2_{L^2(I,H_0^1)} \le \frac{1}{\delta\tau^2} C \left(\|(y_k^h - y_s^h)\|^4_{L^4(I;H_0^1)} + \|(y_{k-1}^h - y_s^h)\|^4_{L^4(I;H_0^1)} \right) \\ + 2\frac{1}{\delta\tau^2}(T\,\|(u_j)\|^2_{L^2(I;\mathbb{R})} + 1) \sum_{i=l+1}^{d} \lambda_i. \quad (42)\end{aligned}$$

We can use the decomposition from [23] as in the section before for the second term in (27):

$$v_k^h - v^h(\tau_k) = \underbrace{v_k^h - P^h v^h(\tau_k)}_{\tilde{\vartheta}_k} + \underbrace{P^h v^h(\tau_k) - v^h(\tau_k)}_{\tilde{\varrho}_k}$$

with the projection $P^h : H_0^1 \to V_h$.

Due to the fact that in this case $\tilde{\varrho}_k = 0$, $\tilde{\vartheta}_0 = 0$ and $\tilde{z}_k = 0$, we find a constant C_ϱ such that

$$\|v_k^h - v^h(\tau_k)\|^2_{L^2(I,H_0^1)} \le C\delta\tau^2 \|y_{tt}^h\|^2_{L^2(I,H_0^1)}. \quad (43)$$

For the third term in (27), there exists by Lemma 4.2 a constant $c(\|u\|_{L^2})$ such that

$$\|(y^h(\tau_k) - y(\tau_k))\|^2_{L^2(I,H_0^1)} \le c(\|u\|_{L^2}) \left(h + \inf_{w_h \in V_h} \|\overline{y} - \overline{y}^h - w^h\| \right).$$

■

We would like to comment on how the term $1/\delta\tau^2$ can be avoided in the estimate. For this purpose we include difference quotients into our snapshot set (39)

$$\tilde{W}_h = \operatorname{span}\{s_0^h, \ldots, s_{2n+1}^h, \overline{\partial}_\tau s_1^h, \ldots, \overline{\partial}_\tau s_{2n+1}^h\}. \quad (44)$$

Instead of (18), we are able to utilize the estimate

$$\sum_{j=0}^{2n+1}\alpha_j\|s_j^h-\sum_{i=1}^{l}(s_j^h,\phi_i)_W\phi_i\|_W^2+\sum_{j=1}^{2n+1}\alpha_j\|\overline{\partial}_\tau s_j^h-\sum_{i=1}^{l}(\overline{\partial}_\tau s_j^h,\phi_i)_W\phi_i\|_W^2=\sum_{i=l+1}^{d}\lambda_i.$$

A straightforward modification of Lemma 6.2 yields the following result.

LEMMA 6.5 *Let V_l, P^l and λ_i be as in section 6.3.1 but for the snapshot set $\bar{W}_h$ in (44). Then for any solution of (37) one has*

$$\begin{aligned}\|\overline{\partial}_\tau(\tilde{y}_k^h-y_{a,k}^h)-P^l\overline{\partial}_\tau(\tilde{y}_k^h-y_{a,k}^h)\|_{H_0^1}^2&\le 2\|(u_j)\|_{L^2(I;\mathbb{R})}^2\sum_{i=l+1}^{d}\lambda_i\\&\quad+2\|u_{k+1}(w_1^h-P^lw_1^h))\|_{H_0^1}^2,\\\|(\overline{\partial}_\tau y_{a,k}^h-P^l(\overline{\partial}_\tau y_{a,k}^h)\|_{L^2(I;H_0^1)}^2&\le\sum_{i=l+1}^{d}\lambda_i.\end{aligned}$$

We introduce the constant

$$c_P'=\sup_{0\neq w^h\in V_h}\frac{\sup_{\|\phi^h\|_{V_l}=1}((\mathrm{id}-P^l)w^h,\phi^h)_{L^2}}{\sup_{\|\phi^h\|_{V_l}=1}(w^h,\phi^h)_{L^2}}.$$

Then we obtain the following corollary for the snapshot set including the difference quotients.

COROLLARY 6.6 *If the snapshots set is taken as in (44), then*

$$\begin{aligned}\|(y_k^l-y(\tau_k))\|_{L^2(I,H_0^1)}^2\le C_1\Big[&\|v_0^l-P^lv^h(\tau_0)\|_{L^2}^2+\delta\tau\nu\|v_0^l-P^lv^h(\tau_0)\|_{H_0^1}^2\\&+(2+\|y_s^h\|_{H_0^1}^2)\left(\|(y_k^h-y_s^h)\|_{L^4(I;H_0^1)}^4+\|(y_{k-1}^h-y_s^h)\|_{L^4(I;H_0^1)}^4\right)\\&+(6T\,\|(u_k)\|_{L^2(I;\mathbb{R})}^2+5)\sum_{i=l+1}^{d}\lambda_i\\&+2\|(u_k)\|_{L^2(I,\mathbb{R})}^2\|w_1^h-P^lw_1^h\|_{H_0^1}^2\Big]\\&+C_2\delta\tau^2\|y_{tt}^h\|_{L^2(I,H_0^1)}^2+c(\|u\|_{L^2})\left(h+\inf_{\phi_h\in V_h}\|\overline{y}-\overline{y}^h-\phi^h\|\right).\end{aligned}$$

Proof We replace the estimate $(z_k,\vartheta_k)_{L^2}\le\|z_k\|_{L^2}\|\vartheta_k\|_{L^2}$ by a refined version.

Let y_k^h and $\tilde{y}_k^h$ be the solutions of (36) and (37), respectively. We have $z_k=\overline{\partial}_\tau v_k^h-P^l\overline{\partial}_\tau v_k^h=\overline{\partial}_\tau y_k^h-P^l\overline{\partial}_\tau y_k^h$. Hence, we obtain for arbitrary $\phi^h\in V_h$

$$\begin{aligned}(z_k,\phi^h)_{L^2}&=(\overline{\partial}_\tau y_k^h-P^l\overline{\partial}_\tau y_k^h,\phi^h)_{L^2}\\&=((\mathrm{id}-P^l)(\overline{\partial}_\tau y_k^h-\overline{\partial}_\tau\tilde{y}_k^h),\phi^h)_{L^2}+(\overline{\partial}_\tau\tilde{y}_k^h-P^l\overline{\partial}_\tau\tilde{y}_k^h,\phi^h)_{L^2}.\end{aligned}$$

In order to invoke Lemma 6.5 the second term can be estimated by

$$(\overline{\partial}_\tau \tilde{y}_k^h - P^l \overline{\partial}_\tau \tilde{y}_k^h, \phi^h)_{L^2} \leq \|\overline{\partial}_\tau \tilde{y}_k^h - P^l \overline{\partial}_\tau \tilde{y}_k^h\|_{H_0^1} \|\phi^h\|_{L^2}$$

We consider next $((\overline{\partial}_\tau y_k^h - \overline{\partial}_\tau \tilde{y}_k^h), \phi^h)_{L^2}$. With $e_k^h := y_k^h - \tilde{y}_k^h$ and $r_k^h := y_k^h - y_s^h$ we have as in the proof of Lemma 6.3

$$(\overline{\partial}_\tau e_k^h, \phi^h) = -\nu(\nabla e_k^h, \nabla \phi^h) - \left\langle (B(e_{k-1}^h, y_s^h) - B(y_s^h, e_k^h), \phi^h \right\rangle - \left\langle B(r_{k-1}^h, r_k^h), \phi^h \right\rangle.$$

The terms on the right hand side can be estimated as follows.

$$\begin{aligned}
|\nu(\nabla e_k^h, \nabla \phi^h)| &\leq \nu \|e_k^h\|_{H_0^1} \|\phi^h\|_{H_0^1}, \\
\left| \left\langle (B(e_{k-1}^h, y_s^h) - B(y_s^h, e_k^h), \phi^h \right\rangle \right| &\leq c_B \|y_s^h\|_{H_0^1} (\|e_{k-1}^h\|_{H_0^1} + \|e_k^h\|_{H_0^1}) \|\phi^h\|_{H_0^1}, \\
\left| \left\langle B(r_{k-1}^h, r_k^h), \phi^h \right\rangle \right| &\leq c_B \|r_{k-1}^h\|_{H_0^1} \|r_k^h\|_{H_0^1} \|\phi^h\|_{H_0^1}.
\end{aligned}$$

We conclude that for all $c_1 > 0$

$$\begin{aligned}
(\overline{\partial}_\tau e_k^h, \phi^h) \leq \frac{\nu}{c_1} \|\phi^h\|_{H_0^1}^2 + c_1 c_2 \Big(&(1 + c_3 \|y_s^h\|_{H_0^1}^2)(\|e_{k-1}^h\|_{H_0^1}^2 + \|e_k^h\|_{H_0^1}^2) \\
&+ c_4 \|r_{k-1}^h\|_{H_0^1}^2 \|r_k^h\|_{H_0^1}^2 \Big).
\end{aligned}$$

Combining both estimates, we arrive at

$$\begin{aligned}
(z_k, \phi^h)_{L^2} \leq \|\overline{\partial}_\tau \tilde{y}_k^h - P^l \overline{\partial}_\tau \tilde{y}_k^h\|_{H_0^1} \|\phi^h\|_{L^2} + c_P' \frac{\nu}{c_1} \|\phi^h\|_{H_0^1}^2 \\
+ c_P' c_1 c_2 \Big((1 + c_3 \|y_s^h\|_{H_0^1}^2)(\|e_{k-1}^h\|_{H_0^1}^2 + \|e_k^h\|_{H_0^1}^2) + c_4 \|r_{k-1}^h\|_{H_0^1}^2 \|r_k^h\|_{H_0^1}^2 \Big).
\end{aligned}$$

We now modify the proof of Lemma 6.1 by using the above estimate for the term $(z_k, \vartheta_k)_{L^2}$ together with Lemma 6.5 and (41) and obtain instead of (28)

$$\begin{aligned}
\|(\vartheta_k)\|_{L^2(I,H_0^1)}^2 \leq C_\vartheta \Big(&\|\vartheta_0\|_{L^2}^2 + \delta\tau\nu \|\vartheta_0\|_{H_0^1}^2 \\
&+ (1 + \|y_s^h\|_{H_0^1}^2)) \left(\|(r_k^h)\|_{L^4(I,H_0^1)}^4 + \|(r_{k-1}^h)\|_{L^4(I,H_0^1)}^4 \right) \\
&+ (6T \|(u_k)\|_{L^2(I,\mathbb{R})}^2 + 5) \sum_{i=l+1}^{d} \lambda_i \\
&+ 2 \|(u_k)\|_{L^2(I,\mathbb{R})}^2 \|w_1^h - P^l w_1^h\|_{H_0^1}^2 \Big).
\end{aligned}$$

The claim follows by using this estimate of ϑ_k instead of (28) in the proof of Theorem 6.4. ∎

Remark 3 The term $\|w_1^h - P^l w_1^h\|_{H_0^1}^2$ can be avoided by including an orthogonolized w_1^h in the POD basis.

Remark 4 Theorem 6.4 and Corollary 6.6 yield error estimates for $\|(y_k^l - y(\tau_k))\|_{L^2(I;H_0^1)}^2$. For objective functionals of the form (6) this leads to an error estimate of the form $O(\|1\|_{L^2(\Omega_o)}^2/\delta\tau^2)\|(y_k^l - y(\tau_k))\|_{L^2(I;H_0^1)}$. An improved

estimate without the factor $1/\delta\tau^2$ can by obtained for objective funtionals of the form

$$J_T(y,u) = \int_0^T (\psi^h, y_t(\cdot,t))^2_{L^2(\Omega)} dt + \frac{\alpha}{2}\int_0^T |u(t)|^2 dt.$$

if $\psi^h \in V_l$. In fact, the identity (29) can be used to estimate the error $(\psi^h, \overline{\partial}_\tau y(\cdot,\tau_k))^2_{L^2(\Omega)} - (\psi^h, \overline{\partial}_\tau y_k^l))^2_{L^2(\Omega)}$ in terms of $\|y_k^l - y(\tau_k)\|^2_{H_0^1}$.

7. POD-based Model Predictive Control

We review the Model Predictive Control approach and describe our numerical procedure to solve the optimal control problem.

7.1. *Model Predictive Control*

For large system dimension as they arise from the discretization of partial differential equations, the effort to solve the optimal control problem for a large time horizon T is enormous. Model Predictive Control provides numerically computable control laws, even for systems of large dimension, see [4, 7, 10, 16] for example.

The approach is based on a time discretization of (21). We consider the semi-implicit Euler method as in section 4.2. The state y of the given controlled process and the corresponding ROM representative β are measured at these discrete time instances. Additionally, at each instant a control input $u(t)$ is selected which influences the future dynamic behavior of the system.

The discretized optimal control problem

$$\begin{aligned} &\min \quad J_T(\beta,u) \\ &\text{subject to} \\ &\tfrac{1}{\delta\tau}M(\beta_{j+1}-\beta_j) + \nu A\beta_{j+1} + n(\beta_j,\beta_{j+1}) = F(u_j) + r, \quad \forall j = 0,\dots,m \\ &\beta(0) = \beta_0, \end{aligned}$$

for $\beta_j = \beta(\tau_j)$ has to be solved over the time horizon T.

The idea of MPC is to replace the optimal control problem on the full time horizon by a sequence of optimal control problems on short control horizons that move forward in time. At each state-time pair (β^*, τ_i) the following finite horizon optimal control problem is solved:

$$\begin{aligned} &\min \quad J_N(\beta,u) \\ &\text{subject to} \\ &\tfrac{1}{\delta\tau}M(\beta_{j+1}-\beta_j) + \nu A\beta_{j+1} + n(\beta_j,\beta_{j+1}) = F(u_j) + r, \quad \forall j = i,\dots,i+N \\ &\beta_i = \beta^*, \end{aligned} \tag{45}$$

with $N \ll m$ and

$$J_N(\beta,u) = \|(\overline{\partial}_\tau \Phi\beta_{j+1})\|^2_{L^2([\tau_i,\tau_{i+N}],\Omega_o)} + \frac{\alpha}{2}\|(u_j)\|^2_{L^2([\tau_i,\tau_{i+N}],\mathbb{R})}.$$

Based on measurements at time τ_i one predicts the future dynamic behavior of the system over a prediction horizon of length N. By optimizing an objective function we obtain a corresponding optimal control sequence. Due to disturbances and

model-plant mismatch, the true system behavior is different from the predicted behavior. In order to incorporate some feedback mechanism, only the first K steps of the optimal control sequence are applied to the system until the next measurement of the state at τ_{i+K+1} becomes available. K is referred to as control horizon. Now the method is repeated with shifted horizon and current state β_{i+K+1}.

We are using an NMPC scheme without terminal costs and constraints. For a discussion of constrained and unconstrained NMPC schemes, see [14]. We will see in the numerical results that for our choice of N the algorithm provides the desired performance.

7.2. *Optimization*

The reduced optimization problem of (45) at each state-time pair (β^*, τ_i) is given by

$$\min \quad \hat{J}(u) := J_N(\beta(u), u),$$

where $\beta(u)$ is the solution of the reduced Navier-Stokes system

$$E(\beta_{j+1}, \beta_j, u_j) = \frac{1}{\delta\tau} M(\beta_{j+1} - \beta_j) + \nu A\beta_{j+1} + n(\beta_j, \beta_{j+1}) - F(u_j) - r$$

for all $j = i, \dots, i+N$ and fulfills the initial conditions.

We are using the adjoint representation of the derivative in the Euclidean space

$$\nabla \hat{J}(u) = E_u^T \lambda + J_u^T,$$

where the adjoint state λ solves the adjoint equation

$$E_\beta^T \lambda = -J_\beta^T.$$

The gradient representation in the correct space is then obtained by choosing the initial BFGS-matrix H_0 accordingly.

We can finally formulate the POD-based Model Predictive Control Algorithm.

Algorithm 1 POD-based Model Predictive Control Algorithm

(1) Choose a prediction horizon of length N and a control horizon of length K.
(2) Given at time τ_0 an initial state β_0, set $j = 0$.
(3) Given initial $u^{(j)} = [u_0^{(j)}, \dots, u_N^{(j)}]$ apply BFGS-method until convergence:
    For $k = 0, 1, \dots$:
    - Solve ROM state equation with $u = u^{(j)}$ and initial value β_j over $[\tau_j, \tau_{j+N}]$.
    - Solve ROM adjoint equation and obtain the adjoint λ_j.
    - Set $\nabla \hat{J}(u^{(j)}) = J_u^T(\beta, u^{(j)}) + E_u^T \lambda_j$.
    - If $\|\hat{J}'(u^{(j)})\|_2 \leq \varepsilon$: goto 3 with result $u^{(j)}$.
    - Compute with BFGS method search direction s_k, step size α_k and update $u^{(j)} = u^{(j)} + \alpha_k s_k$.
(4) Solve state equation with $u = u^{(j)}$ and initial value β_j over $[\tau_j, \tau_{j+K}]$. Obtain new β_{j+K+1}.
(5) Set $j = j + K + 1$. Goto 3.

The control sequence that has to be optimized, is time dependent and has length N of the prediction horizon, which makes in our setting the BFGS approach less

affordable due to memory constraints. Instead we are using a limited memory BFGS method [6].

Additionally, the control amplitude is not allowed to adopt negative values. A negative control amplitude means a negative body force, which the plasma actuator is not able to produce. The optimization algorithm has to be adjusted to bound constraints. To solve the optimization problem with simple constraints we extended the LBFGS, as described in [19].

The initial BFGS matrix is chosen to be

$$H_0 = \alpha \cdot I,$$

which is up to a factor the Hessian of the L^2-regularization. The LBFGSB algorithm terminates if $\|\hat{J}'(u^{(j)})\|_2$ is smaller than a given tolerance ε, a maximum of iteration steps is reached, or additional termination constraints for the control u and the objective J hold

$$\|\alpha_k s_k\|_2 \leq \varepsilon_u, \qquad |J_{k+1} - J_k| \leq \varepsilon_J.$$

8. Numerical Results

Here we present numerical computations related to the approaches presented in the previous paragraphs.

8.1. *Computational Domain*

The computational domain is sketched in (Figure 2). The flat plate is located in $x = [0, 0.7]$. The excitation domain Ω_a starts in $x = 0.225$, the control domain Ω_c in $x = 0.345$, and the sensor domain is located around $(0.395, 0.0005)$.

The flow is considered with an incoming flow velocity $u_\infty = 10$ m/s, kinematic viscosity $\nu = 1.474e{-}5$, length of the flat plate $L = 0.7$ m, and a resulting Reynolds number of $Re \approx 10^6$. The time step size is chosen equidistantly with $\delta\tau = 1e - 5$.

The domain is discretized with Taylor-Hood Finite Elements on a grid of 250 000 nodes. The Finite Element solutions are used for the generation of snapshots and later for comparison with POD reduced-order solutions.

8.2. *POD Validation*

As already described in section 5.3.1 and additionally following Noack et al. [25], who suggest 6 minimum requirements for control-oriented models, we build our snapshot ensemble from a combination of the following cases:

(a) Snapshots of the "uncontrolled" flow y_a, meaning that Tollmien-Schlichting waves are artificial excited in the flow, but there is no control induced by the plasma actuator. 200 snapshots are recorded at constant time intervals $\delta t = 20\delta\tau$, so that the information of four periodic Tollmien-Schlichting periods are contained. In order to obtain the fluctuation, the mean flow $\overline{y}^h$ is subtracted from the snapshots.

(b) Snapshots of the impulse response w. The FEM simulation is carried out without artificial excitation and control, but with initial value $y(0) = y_s + \epsilon \cdot g(x)$, as described in section 5.3.1. The simulation ends if the steady state y_s is reached again. This set consists of 500 snapshots taken at constant time intervals $\delta t = 20\delta\tau$. In this case the steady state y_s is subtracted from the impulse response snapshots to obtain the fluctuation.

With these 700 snapshots, the POD basis is calculated - described in section 5.1 - with $\delta = 99.99\%$. This results in 56 POD basis elements.

Following Noack et al. [26] and as described in section 6.3.1, we add the orthogonalized shift mode, an additional vector describing the mean-field correction between the natural mean flow $\overline{y}^h$ and the steady solution y_s.

In order to validate the reduced order model of dimension 57, the reduced prediction of the snapshots cases is performed. In (Figure 3) and 4 the flow computations with FEM solution are compared to the reduced-order solution over time for the velocity in the middle of the sensor domain Ω_o.

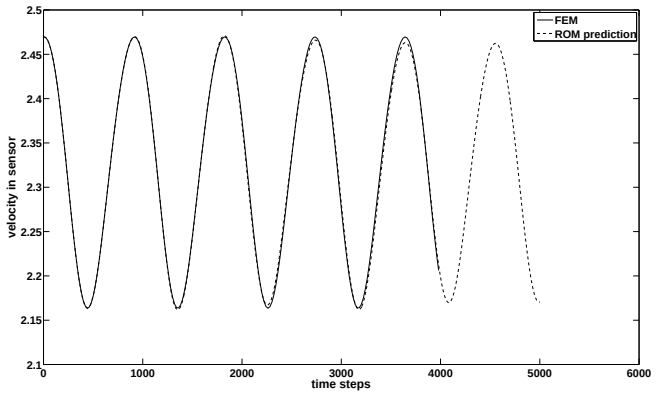

Figure 3. Comparison of velocity values in the middle of Ω_o for the "uncontrolled" case: Tollmien-Schlichting waves are artificially excited in the flow, but there is no control induced by the plasma actuator.

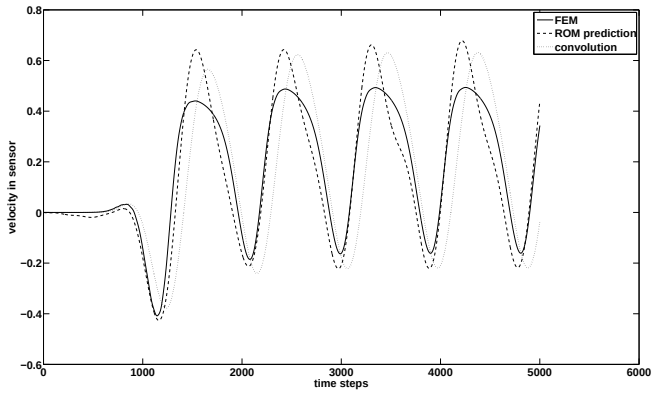

Figure 4. Comparison of velocity values in the middle of Ω_o for a controlled case: no excitation of Tollmien-Schlichting waves, but the plasma actuator generates a sinusoidal control.

(Figure 3) shows the velocity values in the "uncontrolled" case: Tollmien-Schlichting waves are artificially excited, but the plasma actuator induces no control. The comparison of the FEM and the ROM solution shows very good agreement.

The "controlled" case can be seen in (Figure 4). Starting in the steady state, there is no excitation of Tollmien-Schlichting waves, but the plasma actuator generates a sinusoidal control. Additionally to the velocity values of the FEM simulation and the ROM prediction, the convolution is plotted. Due to the linearization around the steady state in the generation of the impulse response snapshots, the convolution as well as the ROM model are lacking some nonlinear information which can be seen in the higher amplitudes. Nevertheless, the describing effect agrees and we

can assume that the reduced model performance is acceptable for the purposes of our controller design.

8.3. *Cancellation Results*

We show the numerical results obtained by solving the optimal control problem (7) with Algorithm 1.

We define as optimization variable the time-dependent amplitude of the force, see (2).

The length of the prediction horizon is chosen to be of size $2000\delta\tau$. One Tollmien-Schlichting wavelength has the length $909\delta\tau$ and the travelling wave needs nearly one wavelength to travel from the actuator to the sensor domain. Therefore we need two times the wavelength in order to measure a complete influenced wave in the sensor domain.

The objective function evaluation is conducted only in the second half of the prediction horizon because of the just mentioned reason. The plasma actuator cannot have an significant effect on the flow, that has already passed the actuator. Therefore, the first measured wavelength in the sensor is not influenced anymore. It might be seen as constant and is neglected in the objective function evaluation.

The control horizon is chosen to be of length $1000\delta\tau$ due to the fact that the control at the actuator over the first wavelength leads to a cancellation in the sensor domain in the second wavelength.

The optimization algorithm is performed with ten MPC steps. The optimization is stopped if the gradient norm is smaller than $\varepsilon = 0.0001$, the change in the control or the objective is smaller than $\varepsilon_u = \varepsilon_J = 0.01$, or the iteration counter exceeds 100. We allowed that the control only varies in $[0, 1]$.

The resulting velocity values in the middle of the sensor area Ω_o can be found in (Figure 5). As comparison the values for the uncontrolled case are plotted. The Tollmien-Schlichting wave with an amplitude of 3% of the inflow velocity can be cancelled within 3000 iterations, respectively 3 optimization steps. Afterwards the cancellation can be maintained. The mean velocity is increasing due to the applied positive body force, which leads to an acceleration of the flow.

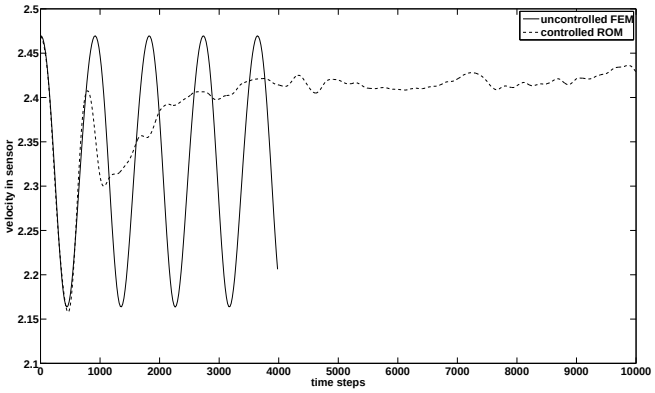

Figure 5. Velocity in the middle of Ω_o - Comparison uncontrolled and controlled

In (Table 1) the underlying convergence history can be found. The objective function value could be reduced in each MPC iteration from J_{old} to J_{new}. The number of needed LBFGSB iterations varies between 7 and 21, which results from either the termination constraint for the objective function or for the control.

Table 1. Iteration history.

MPC it	J_{old}	J_{new}	# BFGS it	termination
1	55.89	0.94	17	$\|\Delta J\|$
2	46.82	0.15	21	$\|\Delta J\|$
3	45.36	0.14	13	$\|\Delta J\|$
4	40.50	0.31	8	$\|\Delta J\|$
5	30.22	0.06	10	$\|\alpha s\|$
6	29.05	0.05	9	$\|\alpha s\|$
7	25.78	0.21	7	$\|\Delta J\|$
8	21.63	0.10	8	$\|\Delta J\|$
9	27.39	0.08	12	$\|\alpha s\|$
10	35.16	0.15	11	$\|\Delta J\|$

The optimized control sequence can be found in (Figure 6). The applied body force in the control area Ω_c is operated nearly periodically, which is not surprising because of the periodic Tollmien-Schlichting waves.

The optimized control sequence $u_k^{(opt)}$ in the MPC iteration k is applied over the control horizon, which means over the first 1000 time steps. The next MPC iteration $k+1$ starts with a control sequence defined by $u_{k+1} = [u_k^{(opt)}(\text{2nd half}), u_k^{(opt)}(\text{2nd half})]$. Additionally, we are passing the updated BFGS matrix H_k as initial BFGS matrix in the next MPC iteration.

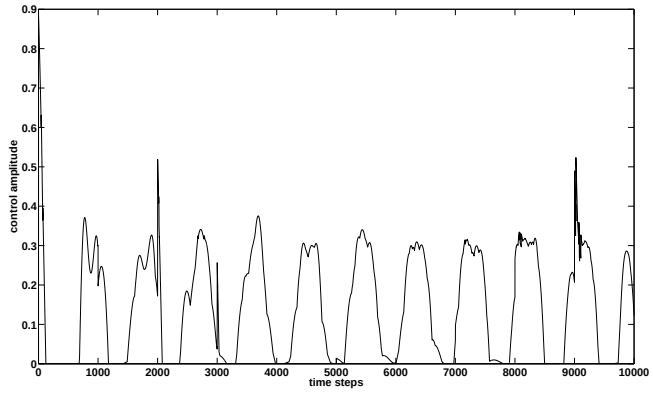

Figure 6. Optimized control amplitude.

The optimized control sequence is then tested in the Finite Element model and the result can be found in (Figure 7). One can see that the optimized control

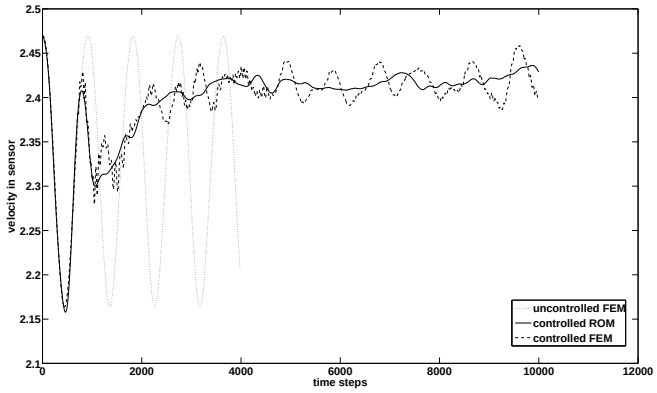

Figure 7. Velocity in in the middle of Ω_o - FEM cancellation result.

sequence developed in the reduced order model is able to lead to a cancellation of

the Tollmien-Schlichting wave also in the FEM. Most of the behavior is represented correctly except of some smaller oscillations.

9. Conclusion

We have introduced a reduced-order model approach using POD, which is, due to the choice of the snapshot basis, suitable for predictions of the state under control. The snapshots ensemble consists of uncontrolled and impulse response snapshots. The advantage is that the POD basis can be generated beforehand and an expensive adjustment of the POD basis during the optimization can be avoided.

We have present a corresponding a-priori error estimate which is applicable to systems under control. By iterating our approach, a snapshot set can be generated that leads to higher order remainder terms. We will study this in future work.

The new ROM approach turns out to be very efficient with respect to our numerical example - the cancellation of Tollmien-Schlichting waves by plasma actuators. The optimization is carried out with an MPC strategy which allows for feedback control such that the control sequence is constantly adjusted to the actual flow configuration.

Acknowledgments

The work of Jane Ghiglieri and Stefan Ulbrich is supported by the 'Excellence Initiative' of the German Federal and State Governments and the Graduate School of Computational Engineering at Technische Universität Darmstadt. Moreover, Stefan Ulbrich was in parts supported by the Cluster of Smart Interfaces and the DFG Priority Programme SPP 1253.

References

[1] K. Afanasiev and M. Hinze, *Adaptive control of a wake flow using proper orthogonal decomposition*, Preprint No. 648 (1999).
[2] E. Arian, M. Fahl, and E.W. Sachs, *Trust-Region Proper Orthogonal Decomposition for Flow Control*, Tech. rep., NASA Langley Research Center, 2000.
[3] C. Bernardi and G. Raugel, *A conforming finite element method for the time-dependent Navier-Stokes equations*, SIAM J. Numer. Anal. 22 (1985), pp. 455–473, URL `http://dx.doi.org/10.1137/0722027`.
[4] T.R. Bewley, P. Moin, and R. Temam, *DNS-based predictive control of turbulence: an optimal benchmark for feedback algorithms*, Journal of Fluid Mechanics 447 (1999), pp. 179–225.
[5] S.C. Brenner and L.R. Scott, Texts in Applied Mathematics, Vol. 15, Springer-Verlag, New York 1994.
[6] R.H. Byrd, P. Lu, J. Nocedal, and C. Zhu, *A Limited Memory Algorithm for Bound Constrained Optimization* (1994).
[7] Y. Chang and S.S. Collis, *Active Control of turbulent channel flows based on Large Eddy Simulation*, in *ASME Paper*, 1999.
[8] S. Chaturantabut and D.C. Sorensen, *Nonlinear Model Reduction via Discrete Empirical Interpolation*, SIAM J. Scientific Computing 32 (2010), pp. 2737–2764.
[9] S. Chaturantabut and D.C. Sorensen, *A State Space Error Estimate for POD-DEIM Nonlinear Model Reduction*, SIAM J. Numerical Analysis 50 (2012), pp. 46–63.
[10] H. Choi, M. Hinze, and K. Kunisch, *Instantaneous control of backward-facing step flows*, Applied Numerical Mathematics 31 (1997).
[11] R.S. de Quadros, *Numerical Optimization of Boundary-Layer Control using Dielectric Barrier Discharge Plasma Actuators*, Dissertation, Technische Universität Darmstadt (2009).
[12] F. Diwoky and S. Volkwein, *Nonlinear boundary control for the heat equation utilizing proper orthogonal decomposition*, in *Fast solutions of Discretized Optimization Problems*, Internat. Ser. Numer. Math. 138, Birkhäuser, Basel, 2001, pp. 73–87.
[13] S. Grundmann, *Transition Control using Dielectric Barrier Discharge Actuators*, Dissertation, Technische Universität Darmstadt (2008).
[14] L. Grüne and J. Pannek, Springer, London 2011.
[15] J.G. Heywood and R. Rannacher, *Finite element approximation of the nonstationary Navier-Stokes problem. I. Regularity of solutions and second-order error estimates for spatial discretization*, SIAM J. Numer. Anal. 19 (1982), pp. 275–311, URL `http://dx.doi.org/10.1137/0719018`.

[16] M. Hinze, *Optimal and instantaneous control of the instationary Navier-Stokes equations*, Institut für Numerische Mathematik, Technische Universität Dresden (2002).
[17] M. Hinze and K. Kunisch, *On Suboptimal Control Strategies for the Navier-Stokes Equations*, ESAIM: Proceedings, Vol. 4 (1998).
[18] M. Hinze, R. Pinnau, M. Ulbrich, and S. Ulbrich, Mathematical Modelling: Theory and Applications, Vol. 23, Springer, New York 2009.
[19] C. Kelley, Society for Industrial and Applied Mathematics 1987, URL `http://books.google.de/books?id=Bq6VcmzOe1IC`.
[20] J. Kriegseis, *Performance Characterization and Quantification of Dielectric Barrier Discharge Plasma Actuators*, Dissertation, Technische Universität Darmstadt (2011).
[21] K. Kunisch and S. Volkwein, *Control of the Burgers equation by a reduced-order approach using proper orthogonal decomposition*, J. Optim. Theory Appl. 102 (1999), pp. 345–371.
[22] K. Kunisch and S. Volkwein, *Crank-Nicolson Galerkin Proper Orthogonal Decomposition Approximations for a General Equation in Fluid Dynamics*, 18th GAMM Seminar on Multigrid and related methods for optimization problems, Leipzig (2002), pp. 97–114.
[23] K. Kunisch and S. Volkwein, *Galerkin Proper Orthogonal Decomposition Methods for a General Equation in Fluid Dynamics*, SIAM Journal on Numerical Analysis 40 (2002), pp. pp. 492–515.
[24] N. Losse, R. King, M. Zengl, U. Rist, and B. Noack, *Control of Tollmien-Schlichting instabilities by finite distributed wall actuation*, Theoretical and Computational Fluid Dynamics 25 (2011), pp. 167–178.
[25] B.R. Noack, G. Tadmor, and M. Morzynski, *Actuation models and dissipative control in empirical Galerkin models of fluid flows*, in *Proceedings of the American Control Conference*, Vol. 6, 2004, pp. 5722 –5727.
[26] B.R. Noack, K. Afanasiev, M. Morzynski, G. Tadmor, and F. Thiele, *A hierarchy of low-dimensional models for the transient and post-transient cylinder wake*, J. Fluid Mech. 497 (2003), pp. 335–363.
[27] S.S. Ravindran, *Proper Orthogonal Decomposition in Optimal Control of Fluids*, Int. J. Numer. Meth. Fluids 34 (1999), pp. 425–448.
[28] S.S. Ravindran, *Reduced-Order Adaptive Controllers for Fluid Flows Using POD*, Journal of Scientific Computing 15 (2000), pp. 457–478.
[29] S.S. Ravindran, *Control of flow separation over a forward-facing step by model reduction*, in *Computer Methods in Applied Mechanics and Engineering*, 2002, pp. 4599–4617.
[30] C.W. Rowley, *Model reduction for fluids using balanced proper orthogonal decomposition*, International Journal 15 (2005), pp. 997–1013.
[31] L. Sirovich, *Turbulence and the dynamics of coherent structure, Part I-III*, Quarterly of Applied Mathematics, 45:561-590 (1987).
[32] K.Y. Tang, W. Graham, and J. Peraire, *Active Flow Control using a Reduced Order Model and Optimum Control*, Tech. rep., Computational Aerospace Sciences Laboratory, MIT Department of Aeronautics and Astronautics, 1996.
[33] R. Temam, AMS Chelsea Publishing, Providence, RI 2001, theory and numerical analysis, Reprint of the 1984 edition.
[34] M. Ulbrich, *Constrained optimal control of Navier-Stokes flow by semismooth Newton methods*, Systems Control Lett. 48 (2003), pp. 297–311, URL `http://dx.doi.org/10.1016/S0167-6911(02)00274-8`, optimization and control of distributed systems.
[35] S. Volkwein, *Optimal control of a phase-field model using proper orthogonal decomposition*, ZAMM - Journal of Applied Mathematics and Mechanics / Zeitschrift für Angewandte Mathematik und Mechanik 81 (2001), pp. 83–97.